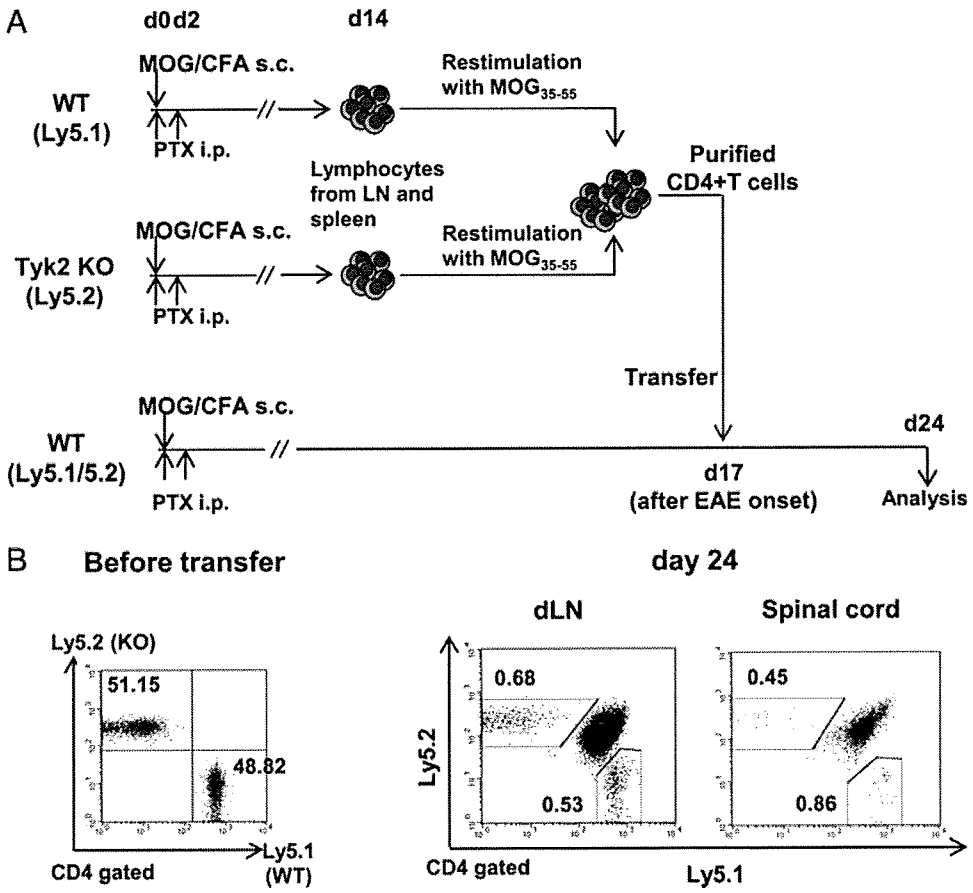

FIGURE 6. Tyk2 KO CD4 T cells were able to infiltrate into the spinal cord of mice developing EAE. *A*, WT (Ly5.1/5.1) and Tyk2-deficient mice (Ly5.2/5.2) were immunized with MOG_{35-55} peptide. On day 14, dLN cells from each group were harvested and restimulated with the peptide for 3 days. A mixture of these effector CD4 T cells was i.v. transferred into WT mice (Ly5.1/5.2) that had been immunized with MOG_{35-55} 17 days previously and that were developing EAE. Seven days after transfer, lymphocytes in dLNs and the spinal cord were analyzed for the profile of donor CD4 T cell populations. *B*, Representative data of flow cytometric analysis are shown after gating on CD4-positive cells.

Discussion

Identification of the key molecule that critically regulates pathogenic T cell responses is important for the development of a novel treatment for autoimmune diseases. EAE is an animal model of MS, in which myelin Ag-specific Th1 and Th17 responses are known to be involved. In the present study, we demonstrated that Tyk2, which is involved in IL-12- and IL-23-signaling, plays important roles in the development of EAE.

Tyk2 participates in signal transduction from multiple cytokine receptors, among which IL-12-signaling has been shown to be highly dependent on Tyk2 (20, 21). We first confirmed in vitro that Tyk2 is critical to IL-12 signaling for the differentiation of Th1 cells. We further found that, although Tyk2 was dispensable for IL-6-signaling for the differentiation of Th17 cells, Tyk2-deficient Th17 cells did not respond to IL-23. Consistent with the results of the in vitro experiments, in vivo development of MOG-specific Th1 cells was greatly reduced in Tyk2-deficient mice. However, normal numbers of MOG-specific Th17 cells were detected in Tyk2 KO mice. This was unexpected because it contradicts the previous reports showing a greatly reduced numbers of MOG-specific Th17 cells in IL-23 KO mice as well as IL-23R KO mice (6, 30, 31). It might be speculated that Tyk2 is indispensable for IL-12 signaling but not for IL-23 signaling in vivo. Jak2, which is another molecule associated with IL-23R and is activated by IL-23 stimulation (23), might compensate for the lack of Tyk2 in IL-23 but not IL-12 signaling, although this does not seem to fully explain the discrepancy between in vivo and in vitro results. Alternatively, defective IL-12-signaling, which drastically reduced Th1 responses in Tyk2 KO mice, might facilitate the development of Th17 cells independently of IL-23 signaling in vivo, as IFN-γ counteracts the differentiation of Th17 cells (7, 32). During the preparation of our manuscript, EAE resistance of Tyk2 mutant B10.D1 mice was reported (33). Although the mechanism for disease resistance was not fully addressed, the authors also found defective IFN-γ production but relatively preserved IL-17A production in CD4 T cells in B10.D1 mice.

Although it was shown that the development of EAE is totally dependent on IL-23, the precise relationship between IL-23 and Th17 in the pathogenesis of EAE remains elusive. Actually, IL-17A is not as essential as IL-23 for the development of EAE, because IL-17A-deficient mice and mice treated with anti-IL-17A mAb developed EAE with mild to even normal severity (2, 34). Additionally, disruption of other Th17-related cytokines, IL-17F and IL-22, did not largely affect the development of EAE (34–36). Although IL-23 can directly act on macrophages as a proinflammatory effector cytokine (3), it unlikely plays predominant roles as evidenced by the normal development of adoptively transferred EAE in IL-23 KO recipients (31). A recent study addressed a role for IL-23 signaling in Th17 cells by using IL-23R KO mice, which were also highly resistant to EAE induction (37). The authors detected fewer IL-23R-deficient CD4 T cells than WT CD4 T cells in the spinal cord of mixed bone marrow chimera mice. From the analysis of OVA-specific TCR transgenic CD4 T cells, it was concluded that IL-23 drove expansion of developing Th17 cells and facilitated their terminal differentiation, which accompanied down-regulation of CD27 and IL-2 and re-up-regulation of the IL-7Rα-chain. Our observation that a significant but reduced number of Tyk2-deficient CD4 T cells infiltrated in the spinal cord of the mixed bone marrow chimera mice is consistent with their data and suggests that the defective IL-23 signaling in Tyk2-deficient Th17 cells accounts for their impaired infiltration. However, we also noted substantial differences in Th17 cells between IL-23R KO

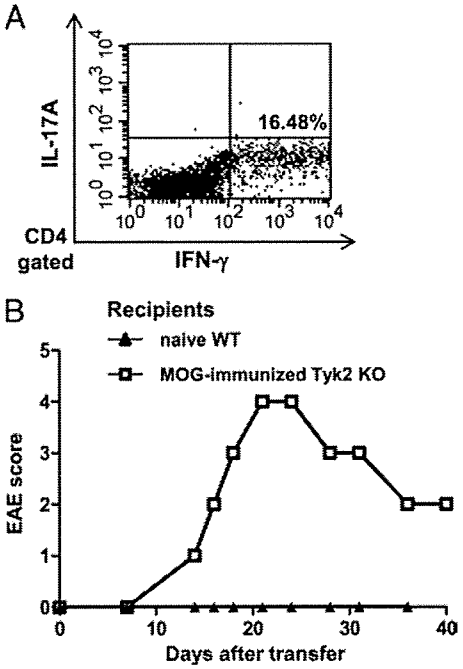

FIGURE 7. EAE was induced in MOG_{35-55}-immunized Tyk2 KO mice by transferring Th1 cells. *A*, Th1 cells were induced from dLN cells of MOG_{35-55}-immunized IL-17A KO mice by culturing under Th1 polarizing condition for 4 days. *B*, Representative EAE score of naive WT mice and MOG_{35-55}-immunized Tyk2 KO mice, both of which were transferred with 1×10^6 of the MOG_{35-55}-primed Th1 cells.

and Tyk2 KO mice. First, as described above, a similar number of Th17 cells were detected in the dLNs of WT and Tyk2 KO mice at day 21, while the number of Th17 cells in the periphery of IL-23R KO mice greatly decreased from day 7 (37). The levels of CD27 expression and IL-2 production were similar in Tyk2 KO and WT CD4 T cells, although expression of the IL-7Rα-chain was slightly decreased in Tyk2 KO CD4 T cells (data not shown). Moreover, Tyk2-deficient Th17 cells were functionally competent, as supplementation of a suboptimal number of WT Th1 cells, which did not induce EAE in naive WT mice, induced EAE in MOG-immunized Tyk2 KO mice. Therefore, the mechanism for EAE resistance might not be identical in Tyk2 KO mice and IL-23 or IL-23R KO mice.

Induction of EAE in MOG-primed Tyk2 KO mice by transferring WT Th1 cells suggests that the diminished Th1 responses in Tyk2 KO mice is also involved in the mechanism for disease resistance. In this regard, the preferential ability of Th1 cells to access a noninflamed CNS, which initiated inflammation to facilitate local entry of Th17 cells, is of particular interest (13). Furthermore, in conflict with the earlier report by Cua et al. (3), Thakker et al. showed that both IFN-γ and IL-17A production was impaired in IL-23p19 KO mice (31). There is also evidence that administration of IFN-γ exacerbated human multiple sclerosis (38). Nevertheless, it is also well known that IFN-γ or IFN-γR KO mice are susceptible to EAE (9–11), although its mechanism remains unknown. It is possible that the absence of IFN-γ signaling might exert effects on the immune system beyond defective Th1 responses. In fact, a role for IFN-γ in the generation of $Foxp3^+$ CD4 regulatory T cells was reported (39). Additionally, a lack of IFN-γ likely results in an overproduction of Th17 cells, which might circumvent the need for Th1 responses. Further studies are needed to elucidate the roles and relationships of Th1 and Th17 cells in various inflammatory conditions in vivo.

Treatment of autoimmune diseases has greatly advanced since the introduction of biological reagents such as anti-TNF-α mAbs. However, given the enormous number of patients with autoimmune diseases, safety and the cost of current injectable protein-based therapies are a matter of concern. Therefore, much attention has been paid more recently on small molecule inhibitors for intracellular cytokine signaling. Jak family kinase is one of the candidate molecules and, in fact, Jak3 inhibitor is already under a clinical trial for the treatment of rheumatoid arthritis (40). Because the relative importance of Th1 and Th17 cells in many autoimmune diseases has not yet been clarified, we propose from our results that Tyk2 could be a candidate target molecule for their treatment. In support of this idea, it was recently reported that Tyk2 was identified as a susceptible factor of human multiple sclerosis (41).

Acknowledgments

We thank Dr. Motozumi Minohara, Kazue Hirowatari, Yoko Tagawa, Akiko Yano, and Kiyomi Akasaki for their excellent technical support.

Disclosures

The authors have no financial conflicts of interest.

References

1. Zamvil, S. S., and L. Steinman. 1990. The T lymphocyte in experimental allergic encephalomyelitis. *Annu. Rev. Immunol.* 8: 579–621.
2. Komiyama, Y., S. Nakae, T. Matsuki, A. Nambu, H. Ishigame, S. Kakuta, K. Sudo, and Y. Iwakura. 2006. IL-17 plays an important role in the development of experimental autoimmune encephalomyelitis. *J. Immunol.* 177: 566–573.
3. Cua, D. J., J. Sherlock, Y. Chen, C. A. Murphy, B. Joyce, B. Seymour, L. Lucian, W. To, S. Kwan, T. Churakova, et al. 2003. Interleukin-23 rather than interleukin-12 is the critical cytokine for autoimmune inflammation of the brain. *Nature* 421: 744–748.
4. Oppmann, B., R. Lesley, B. Blom, J. C. Timans, Y. Xu, B. Hunte, F. Vega, N. Yu, J. Wang, K. Singh, et al. 2000. Novel p19 protein engages IL-12p40 to form a cytokine, IL-23, with biological activities similar as well as distinct from IL-12. *Immunity* 13: 715–725.
5. Ghilardi, N., N. Kljavin, Q. Chen, S. Lucas, A. L. Gurney, and F. J. De Sauvage. 2004. Compromised humoral and delayed-type hypersensitivity responses in IL-23-deficient mice. *J. Immunol.* 172: 2827–2833.
6. Langrish, C. L., Y. Chen, W. M. Blumenschein, J. Mattson, B. Basham, J. D. Sedgwick, T. McClanahan, R. A. Kastelein, and D. J. Cua. 2005. IL-23 drives a pathogenic T cell population that induces autoimmune inflammation. *J. Exp. Med.* 201: 233–240.
7. Park, H., Z. Li, X. O. Yang, S. H. Chang, R. Nurieva, Y. H. Wang, Y. Wang, L. Hood, Z. Zhu, Q. Tian, and C. Dong. 2005. A distinct lineage of CD4 T cells regulates tissue inflammation by producing interleukin 17. *Nat. Immunol.* 6: 1133–1141.
8. Korn, T., E. Bettelli, M. Oukka, and V. K. Kuchroo. 2009. IL-17 and Th17 Cells. *Annu. Rev. Immunol.* 27: 485–517.
9. Ferber, I. A., S. Brocke, C. Taylor-Edwards, W. Ridgway, C. Dinisco, L. Steinman, D. Dalton, and C. G. Fathman. 1996. Mice with a disrupted IFN-γ gene are susceptible to the induction of experimental autoimmune encephalomyelitis (EAE). *J. Immunol.* 156: 5–7.
10. Krakowski, M., and T. Owens. 1996. Interferon-γ confers resistance to experimental allergic encephalomyelitis. *Eur. J. Immunol.* 26: 1641–1646.
11. Willenborg, D. O., S. Fordham, C. C. Bernard, W. B. Cowden, and I. A. Ramshaw. 1996. IFN-γ plays a critical down-regulatory role in the induction and effector phase of myelin oligodendrocyte glycoprotein-induced autoimmune encephalomyelitis. *J. Immunol.* 157: 3223–3227.
12. Kroenke, M. A., T. J. Carlson, A. V. Andjelkovic, and B. M. Segal. 2008. IL-12- and IL-23-modulated T cells induce distinct types of EAE based on histology, CNS chemokine profile, and response to cytokine inhibition. *J. Exp. Med.* 205: 1535–1541.
13. O'Connor, R. A., C. T. Prendergast, C. A. Sabatos, C. W. Lau, M. D. Leech, D. C. Wraith, and S. M. Anderton. 2008. Cutting edge: Th1 cells facilitate the entry of Th17 cells to the central nervous system during experimental autoimmune encephalomyelitis. *J. Immunol.* 181: 3750–3754.
14. Millward, J. M., M. Caruso, I. L. Campbell, J. Gauldie, and T. Owens. 2007. IFN-γ-induced chemokines synergize with pertussis toxin to promote T cell entry to the central nervous system. *J. Immunol.* 178: 8175–8182.
15. Velazquez, L., M. Fellous, G. R. Stark, and S. Pellegrini. 1992. A protein tyrosine kinase in the interferon α/β signaling pathway. *Cell* 70: 313–322.
16. Stahl, N., T. G. Boulton, T. Farruggella, N. Y. Ip, S. Davis, B. A. Witthuhn, F. W. Quelle, O. Silvennoinen, G. Barbieri, S. Pellegrini, et al. 1994. Association and activation of Jak-Tyk kinases by CNTF-LIF-OSM-IL-6β receptor components. *Science* 263: 92–95.
17. Finbloom, D. S., and K. D. Winestock. 1995. IL-10 induces the tyrosine phosphorylation of tyk2 and Jak1 and the differential assembly of STAT1 alpha and

STAT3 complexes in human T cells and monocytes. *J. Immunol.* 155: 1079–1090.
18. Bacon, C. M., D. W. McVicar, J. R. Ortaldo, R. C. Rees, J. J. O'Shea, and J. A. Johnston. 1995. Interleukin 12 (IL-12) induces tyrosine phosphorylation of JAK2 and TYK2: differential use of Janus family tyrosine kinases by IL-2 and IL-12. *J. Exp. Med.* 181: 399–404.
19. Leonard, W. J., and J. J. O'Shea. 1998. Jaks and STATs: biological implications. *Annu. Rev. Immunol.* 16: 293–322.
20. Shimoda, K., K. Kato, K. Aoki, T. Matsuda, A. Miyamoto, M. Shibamori, M. Yamashita, A. Numata, K. Takase, S. Kobayashi, et al. 2000. Tyk2 plays a restricted role in IFNα signaling, although it is required for IL-12-mediated T cell function. *Immunity* 13: 561–571.
21. Karaghiosoff, M., H. Neubauer, C. Lassnig, P. Kovarik, H. Schindler, H. Pircher, B. McCoy, C. Bogdan, T. Decker, G. Brem, et al. 2000. Partial impairment of cytokine responses in Tyk2-deficient mice. *Immunity* 13: 549–560.
22. Shimoda, K., H. Tsutsui, K. Aoki, K. Kato, T. Matsuda, A. Numata, K. Takase, T. Yamamoto, H. Nukina, T. Hoshino, et al. 2002. Partial impairment of interleukin-12 (IL-12) and IL-18 signaling in Tyk2-deficient mice. *Blood* 99: 2094–2099.
23. Parham, C., M. Chirica, J. Timans, E. Vaisberg, M. Travis, J. Cheung, S. Pflanz, R. Zhang, K. P. Singh, F. Vega, et al. 2002. A receptor for the heterodimeric cytokine IL-23 is composed of IL-12Rβ1 and a novel cytokine receptor subunit, IL-23R. *J. Immunol.* 168: 5699–5708.
24. Shaw, M. H., V. Boyartchuk, S. Wong, M. Karaghiosoff, J. Ragimbeau, S. Pellegrini, M. Muller, W. F. Dietrich, and G. S. Yap. 2003. A natural mutation in the Tyk2 pseudokinase domain underlies altered susceptibility of B10.Q/J mice to infection and autoimmunity. *Proc. Natl. Acad. Sci. USA* 100: 11594–11599.
25. Tokumasa, N., A. Suto, S. Kagami, S. Furuta, K. Hirose, N. Watanabe, Y. Saito, K. Shimoda, I. Iwamoto, and H. Nakajima. 2007. Expression of Tyk2 in dendritic cells is required for IL-12, IL-23, and IFN-γ production and the induction of Th1 cell differentiation. *Blood* 110: 553–560.
26. Nakamura, R., K. Shibata, H. Yamada, K. Shimoda, K. Nakayama, and Y. Yoshikai. 2008. Tyk2-signaling plays an important role in host defense against *Escherichia coli* through IL-23-induced IL-17 production by $\gamma\delta$ T cells. *J. Immunol.* 181: 2071–2075.
27. Li, W., H. Yamada, T. Yajima, R. Nakagawa, K. Shimoda, K. Nakayama, and Y. Yoshikai. 2007. Tyk2 signaling in host environment plays an important role in contraction of antigen-specific $CD8^+$ T cells following a microbial infection. *J. Immunol.* 178: 4482–4488.
28. Nakae, S., Y. Komiyama, A. Nambu, K. Sudo, M. Iwase, I. Homma, K. Sekikawa, M. Asano, and Y. Iwakura. 2002. Antigen-specific T cell sensitization is impaired in IL-17-deficient mice, causing suppression of allergic cellular and humoral responses. *Immunity* 17: 375–387.
29. Veldhoen, M., R. J. Hocking, R. A. Flavell, and B. Stockinger. 2006. Signals mediated by transforming growth factor-β initiate autoimmune encephalomyelitis, but chronic inflammation is needed to sustain disease. *Nat. Immunol.* 7: 1151–1156.
30. Murphy, C. A., C. L. Langrish, Y. Chen, W. Blumenschein, T. McClanahan, R. A. Kastelein, J. D. Sedgwick, and D. J. Cua. 2003. Divergent pro- and anti-inflammatory roles for IL-23 and IL-12 in joint autoimmune inflammation. *J. Exp. Med.* 198: 1951–1957.
31. Thakker, P., M. W. Leach, W. Kuang, S. E. Benoit, J. P. Leonard, and S. Marusic. 2007. IL-23 is critical in the induction but not in the effector phase of experimental autoimmune encephalomyelitis. *J. Immunol.* 178: 2589–2598.
32. Harrington, L. E., R. D. Hatton, P. R. Mangan, H. Turner, T. L. Murphy, K. M. Murphy, and C. T. Weaver. 2005. Interleukin 17-producing $CD4^+$ effector T cells develop via a lineage distinct from the T helper type 1 and 2 lineages. *Nat. Immunol.* 6: 1123–1132.
33. Spach, K. M., R. Noubade, B. McElvany, W. F. Hickey, E. P. Blankenhorn, and C. Teuscher. 2009. A single nucleotide polymorphism in Tyk2 controls susceptibility to experimental allergic encephalomyelitis. *J. Immunol.* 182: 7776–7783.
34. Haak, S., A. L. Croxford, K. Kreymborg, F. L. Heppner, S. Pouly, B. Becher, and A. Waisman. 2009. IL-17A and IL-17F do not contribute vitally to autoimmune neuro-inflammation in mice. *J. Clin. Invest.* 119: 61–69.
35. Yang, X. O., S. H. Chang, H. Park, R. Nurieva, B. Shah, L. Acero, Y. H. Wang, K. S. Schluns, R. R. Broaddus, Z. Zhu, and C. Dong. 2008. Regulation of inflammatory responses by IL-17F. *J. Exp. Med.* 205: 1063–1075.
36. Kreymborg, K., R. Etzensperger, L. Dumoutier, S. Haak, A. Rebollo, T. Buch, F. L. Heppner, J. C. Renauld, and B. Becher. 2007. IL-22 is expressed by Th17 cells in an IL-23-dependent fashion, but not required for the development of autoimmune encephalomyelitis. *J. Immunol.* 179: 8098–8104.
37. McGeachy, M. J., Y. Chen, C. M. Tato, A. Laurence, B. Joyce-Shaikh, W. M. Blumenschein, T. K. McClanahan, J. J. O'Shea, and D. J. Cua. 2009. The interleukin 23 receptor is essential for the terminal differentiation of interleukin 17-producing effector T helper cells in vivo. *Nat. Immunol.* 10: 314–324.
38. Panitch, H. S., R. L. Hirsch, A. S. Haley, and K. P. Johnson. 1987. Exacerbations of multiple sclerosis in patients treated with gamma interferon. *Lancet* 1: 893–895.
39. Wang, Z., J. Hong, W. Sun, G. Xu, N. Li, X. Chen, A. Liu, L. Xu, B. Sun, and J. Z. Zhang. 2006. Role of IFN-γ in induction of Foxp3 and conversion of $CD4^+CD25^-$ T cells to $CD4^+$ Tregs. *J. Clin. Invest.* 116: 2434–2441.
40. Kremer, J. M., B. J. Bloom, F. C. Breedveld, J. H. Coombs, M. P. Fletcher, D. Gruben, S. Krishnaswami, R. Burgos-Vargas, B. Wilkinson, C. A. Zerbini, and S. H. Zwillich. 2009. The safety and efficacy of a JAK inhibitor in patients with active rheumatoid arthritis: results of a double-blind, placebo-controlled phase IIa trial of three dosage levels of CP-690,550 versus placebo. *Arthritis Rheum.* 60: 1895–1905.
41. Ban, M., A. Goris, A. R. Lorentzen, A. Baker, T. Mihalova, G. Ingram, D. R. Booth, R. N. Heard, G. J. Stewart, E. Bogaert, et al. 2009. Replication analysis identifies TYK2 as a multiple sclerosis susceptibility factor. *Eur. J. Hum. Genet.* 17: 1309–1313.

THE JOURNAL OF BIOLOGICAL CHEMISTRY VOL. 284, NO. 20, pp. 13766–13777, May 15, 2009

Promotion of Neurite Extension by Protrudin Requires Its Interaction with Vesicle-associated Membrane Protein-associated Protein

Received for publication, October 15, 2008, and in revised form, March 13, 2009 Published, JBC Papers in Press, March 16, 2009, DOI 10.1074/jbc.M807938200

Shotaro Saita[‡§], **Michiko Shirane**[‡§], **Tohru Natume**[¶], **Shun-ichiro Iemura**[¶], **and Keiichi I. Nakayama**[‡§1]

From the [‡]*Department of Molecular and Cellular Biology, Medical Institute of Bioregulation, Kyushu University, 3-1-1 Maidashi, Higashi-ku, Fukuoka, Fukuoka 812-8582, Japan,* [§]*CREST, Japan Science and Technology Corporation, Kawaguchi, Saitama 332-0012, Japan, and the* [¶]*National Institutes of Advanced Industrial Science, Kohtoh-ku, Tokyo 135-0064, Japan*

Protrudin is a protein that contains a Rab11-binding domain and a FYVE (lipid-binding) domain and that functions to promote neurite formation through interaction with the GDP-bound form of Rab11. Protrudin also contains a short sequence motif designated FFAT (two phenylalanines in an acidic tract), which in other proteins has been shown to mediate binding to vesicle-associated membrane protein-associated protein (VAP). We now show that protrudin associates and colocalizes with VAP-A, an isoform of VAP expressed in the endoplasmic reticulum. Both the interaction between protrudin and VAP-A as well as the induction of process formation by protrudin were markedly inhibited by mutation of the FFAT motif. Furthermore, depletion of VAP-A by RNA interference resulted in mislocalization of protrudin as well as in inhibition of neurite outgrowth induced by nerve growth factor in rat pheochromocytoma PC12 cells. These defects resulting from depletion of endogenous rat VAP-A in PC12 cells were corrected by forced expression of (RNA interference-resistant) human VAP-A but not by VAP-A mutants that have lost the ability to interact with protrudin. These results suggest that VAP-A is an important regulator both of the subcellular localization of protrudin and of its ability to stimulate neurite outgrowth.

The molecular mechanisms that underlie neurite formation include both cytoskeletal remodeling and membrane trafficking. Membrane components are transported in a directional manner within the cell by a membrane recycling system, resulting in expansion of the surface area of the neurite. The small GTPase Rab11 regulates membrane recycling and constitutive exocytosis (1), and it is thought to contribute to neurite formation through regulation of directional membrane transport.

We have recently identified protrudin as a key regulator of Rab11-dependent membrane trafficking during neurite extension. Protrudin interacts with FKBP38 (also known as FKBP8) (2), which is a member of the immunophilin family of proteins that bind the immunosuppressant drug FK506 (3). FKBPs are multifunctional proteins that regulate the folding or export of other proteins as a result of their peptidyl-prolyl *cis-trans*-isomerase activity (4). Protrudin was found to interact with FKBP38, but not with other FKBP proteins such as FKBP12 or FKBP52 (5). Protrudin is hyperphosphorylated in *Fkbp38*$^{-/-}$ mice, which manifest abnormal extension of nerve fibers (5).

Protrudin contains a Rab11-binding domain (RBD11), two transmembrane domains (TM1 and TM2),[2] an FFAT (two phenylalanines in an acidic tract) motif (6), a coiled-coil domain, and a FYVE domain (7). These structural characteristics suggested that protrudin might function in membrane trafficking, particularly in membrane recycling. The gene encoding ZFYVE27 (a synonym of human protrudin) was recently found to be mutated in a German family with an autosomal dominant form of hereditary spastic paraplegia (AD-HSP), which is characterized by selective degeneration of axons (8). The phenotype of the affected individuals is similar to that of patients with AD-HSP caused by mutation of spastin, a protein implicated in neuronal vesicular trafficking (9), and protrudin was shown to interact with spastin (8). These findings support the notion that protrudin plays a key role in Rab11-mediated directional membrane transport during neurite formation.

The subcellular localization of protrudin is dynamic. Whereas it is localized to the endoplasmic reticulum (ER) under basal conditions, nerve growth factor (NGF) triggers the translocation of protrudin from the ER, via recycling endosomes, to the tip of membrane protrusions in neuronal cells. Given that the FFAT motif is thought to serve as an ER targeting signal (6), this motif might be expected to contribute both to the localization of protrudin to the ER and to the regulation of neurite formation by this protein. The FFAT motif (consensus amino acid sequence of EFFDA*X*E, where *X* is any amino acid) is present in several lipid-binding proteins that are implicated in the transfer of lipids between the ER and other organelles such as the Golgi apparatus (10, 11). Vesicle-associated membrane protein-associated protein (VAP) interacts with these lipid-binding proteins through their FFAT motifs (6, 11, 12). The VAP-A and VAP-B isoforms of mammalian VAP are ER-resident type II membrane proteins (13) that are encoded by different genes (14); VAP-C is a splicing variant of VAP-B that

[1] To whom correspondence should be addressed: Dept. of Molecular and Cellular Biology, Medical Institute of Bioregulation, Kyushu University, 3-1-1 Maidashi, Higashi-ku, Fukuoka, Fukuoka 812-8582, Japan. Tel.: 81-92-642-6815; Fax: 81-92-642-6819; E-mail: nakayak1@bioreg.kyushu-u.ac.jp.

[2] The abbreviations used are: TM, transmembrane domain; AD-HSP, autosomal dominant hereditary spastic paraplegia; ER, endoplasmic reticulum; NGF, nerve growth factor; VAP, vesicle-associated membrane protein-associated protein; shRNA, short hairpin RNA; MS/MS, tandem mass spectrometry; GST, glutathione S-transferase; HA, hemagglutinin epitope; PDI, protein-disulfide isomerase; PBS, phosphate-buffered saline; MSP, major sperm protein.

TABLE 1

Identification of protrudin-associated proteins by proteomics analysis

HEK293T cells transiently expressing 3× FLAG-tagged human protrudin were subjected to immunoaffinity chromatography with anti-FLAG. Proteins in the column eluate were digested with Lys-C endoproteinase, and the resulting peptide fragments were analyzed directly with a highly sensitive liquid chromatography-MS/MS system. The proteins reproducibly detected in two independent experiments are listed. The percentage of sequence coverage for each protein is also shown.

Protein	Sequence coverage
	%
Vesicle associated membrane protein-associated protein A (VAP-A)	14.5
Vesicle associated membrane protein-associated protein B and C (VAP-B/C)	14.4
T-complex protein 1, δ subunit (TCPD)	9.2
T-complex protein 1, γ subunit (TCPG)	7.7
T-complex protein 1, ϵ subunit (TCPE)	6.3

lacks the membrane-spanning domain. VAP-A and VAP-B share ~60% amino acid sequence identity, form homo- or heterodimers, and are expressed in many tissues (14–16). In addition to their localization to the ER (16), VAP-A and VAP-B are present in a wide range of intracellular membranes or membrane structures, including the Golgi, the ER-Golgi intermediate compartment (17), tight junctions (18), neuromuscular junctions (19), recycling endosomes, and the plasma membrane (20).

We have now identified VAP-A and VAP-B as proteins that interact with protrudin. Protrudin preferentially interacts with VAP-A via its FFAT motif, and this motif was found to be required for the protrudin-dependent formation of membrane protrusions in HeLa cells. In addition, depletion of VAP-A by RNA interference resulted in inhibition of NGF-induced neurite outgrowth in the PC12 rat pheochromocytoma cell line. This inhibition of neurite outgrowth was reversed by expression of human VAP-A but not by that of VAP-A mutants that have lost the ability to bind to protrudin. These results suggest that interaction of protrudin with VAP-A is important both for its ER retention and for its ability to stimulate neurite formation.

EXPERIMENTAL PROCEDURES

Construction of Plasmids—Construction of vectors encoding human protrudin and FKBP52 was described previously (2, 21). Complementary DNAs encoding mutants of protrudin were generated by the PCR with Prime Star polymerase (Takara, Ohtsu, Japan); those encoding VAP-A or VAP-B were generated by PCR from a human kidney cDNA library; and that encoding RAMP4 was generated by PCR from a mouse thyroid cDNA library. The VAP or RAMP4 cDNAs were subcloned into the pEF-BOS-2× HA or pEF-BOS-2× Myc vectors (kindly provided by Shigekazu Nagata, Kyoto University, Japan) or into pGEX-6P (Amersham Biosciences). DNA fragments encoding stem-loop-type short hairpin RNAs (shRNAs) specific for rat VAP mRNAs (VAP-A-shRNA 1, 5′-GGTAGCACATTCGGATAAACC-3′; VAP-A-shRNA 2, 5′-GCCGTGTCCTTCAGAGATAAT-3′; VAP-A-shRNA 3, 5′-GGATTCTTTCTAGGGAAATTC-3′; VAP-B-shRNA 1, 5′-GGGTCATTATAGGGAAGATCG-3′; VAP-B-shRNA 2, 5′-GGTGGTGCTGTTCTTTATTGT-3′; VAP-B-shRNA 3, 5′-GCCCGACACTTCCGATATGGA-3′); or human VAP-B mRNA (5′-GGGAGGAGAACAAGCAGTTCA-3′) were synthesized, attached to the U6 promoter, and subcloned into the vector pIRES-Venus-B (Venus cDNA was kindly provided by Atsushi Miyawaki, RIKEN, Japan), which contains an internal ribosome entry site and encodes the reporter protein Venus.

Protein Identification by Liquid Chromatography-MS/MS Analysis—Human protrudin tagged with the FLAG epitope at its NH_2 terminus was transiently expressed in HEK293T cells

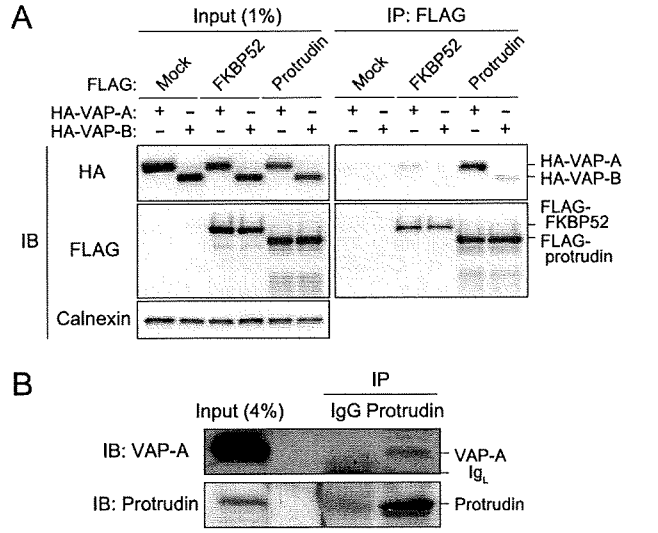

FIGURE 1. **Interaction between protrudin and VAP.** *A*, extracts of HEK293T cells transiently transfected with expression vectors for 3× FLAG-tagged protrudin or FKBP52 (negative control) and for 2× HA-tagged VAP-A or VAP-B were subjected to immunoprecipitation (*IP*) with anti-FLAG. The resulting precipitates, as well as a portion (1% of the input for immunoprecipitation) of the cell extracts, were subjected to immunoblot analysis (*IB*) with anti-HA, anti-FLAG, or anti-calnexin (loading control). *B*, mouse brain extract was subjected to immunoprecipitation with anti-protrudin or control rabbit IgG, and the resulting precipitates, as well as a portion (4% of the input for immunoprecipitation) of the tissue extract, were subjected to immunoblot analysis with anti-VAP-A and anti-protrudin. Ig_L, Ig light chain.

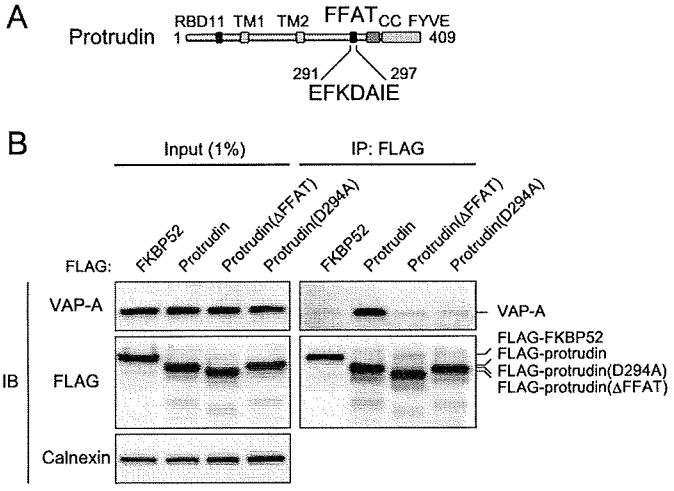

FIGURE 2. **Role of the FFAT motif in the interaction of protrudin with VAP-A.** *A*, domain organization of human protrudin. *B*, extracts of HEK293T cells transiently transfected with an expression vector for 3× FLAG-tagged protrudin, protrudin mutants (ΔFFAT or D294A), or FKBP52 were subjected to immunoprecipitation with anti-FLAG. The resulting precipitates, as well as a portion (1% of the input for immunoprecipitation) of the cell extracts, were subjected to immunoblot analysis with anti-VAP-A, anti-FLAG, or anti-calnexin.

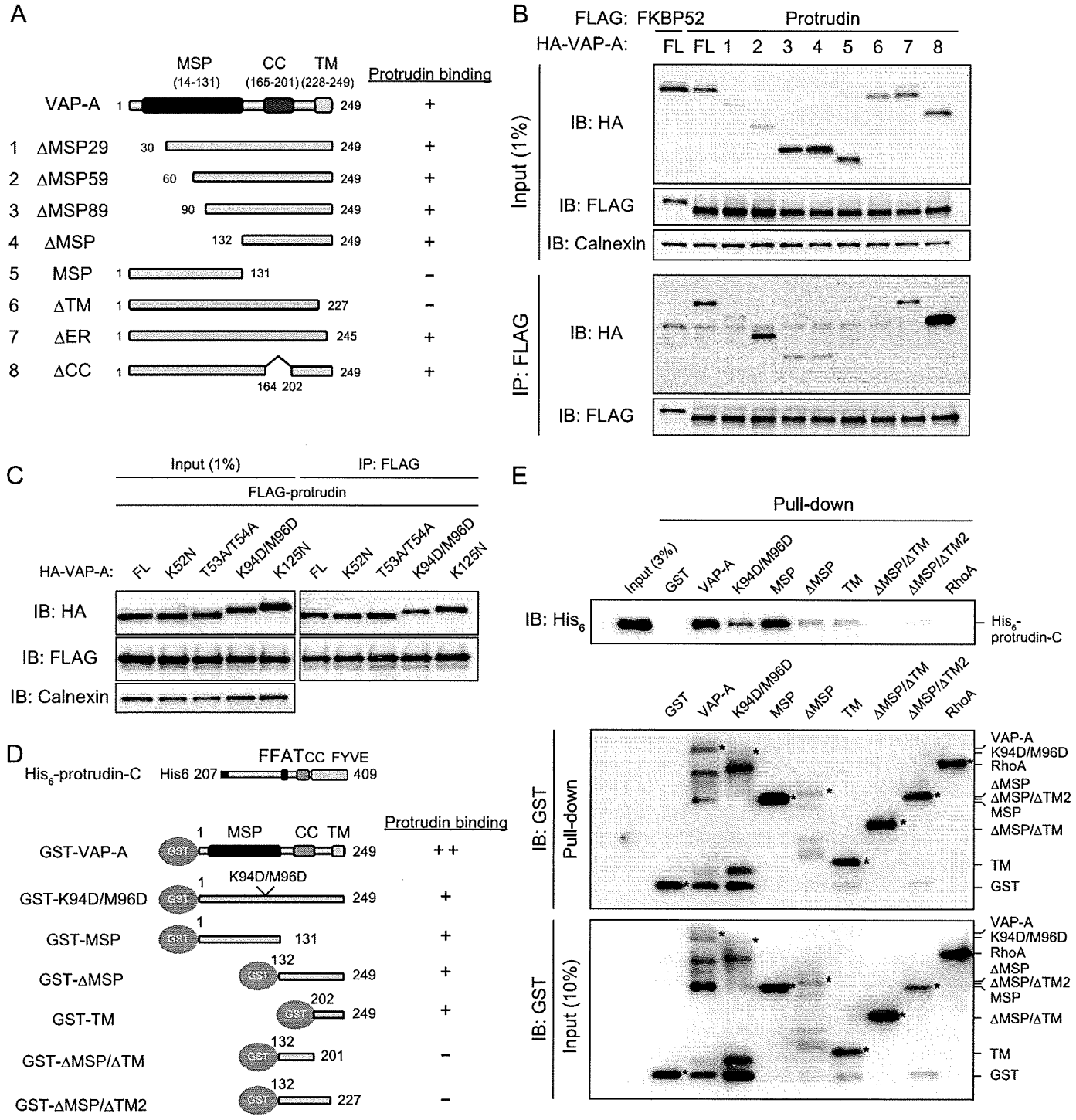

FIGURE 3. **Delineation of the regions of VAP-A responsible for interaction with protrudin.** *A*, domain organization of human VAP-A and structure of deletion mutants thereof. A summary of the ability of the mutants to bind protrudin as determined in *B* is shown on the *right*. *B*, full-length (*FL*) VAP-A or the mutants thereof shown in *A* fused at their NH_2 termini to the 2× HA tag were expressed in HEK293T cells together with 3× FLAG-tagged protrudin or FKBP52. The cell extracts were subjected to immunoprecipitation with anti-FLAG, and the resulting precipitates, as well as a portion (1% of the input for immunoprecipitation) of the cell extracts, were subjected to immunoblot (*IB*) analysis with anti-HA, anti-FLAG, or anti-calnexin. *C*, full-length human VAP-A and the indicated mutants thereof fused at their NH_2 termini to the 2× HA tag were expressed together with 3× FLAG-tagged protrudin in HEK293T cells. The cell extracts were subjected to immunoprecipitation with anti-FLAG, and the resulting precipitates, as well as a portion (1% of the input for immunoprecipitation) of the cell extracts, were subjected to immunoblot analysis with anti-HA, anti-FLAG, or anti-calnexin. *D*, structure of VAP-A mutants fused to GST at their NH_2 termini and a summary of their ability to bind to a His_6-tagged COOH-terminal fragment of protrudin comprising residues 207–409 (protrudin-C) as determined in *E*. *E*, His_6-tagged protrudin-C was incubated with the GST-tagged VAP-A mutants shown in *D* or with GST-RhoA or GST as negative controls, and the binding mixtures were then subjected to precipitation with glutathione-conjugated beads. The bead-bound proteins (*Pull-down*), as well as a portion (3 or 10% of the input for precipitation) of the binding mixtures, were subjected to immunoblot analysis with anti-His_6 and anti-GST. The *asterisks* indicate bands corresponding to the GST-tagged proteins.

and then purified together with associated proteins from cell lysates by immunoaffinity chromatography with anti-FLAG. Protrudin-associated proteins were digested with Lys-C endoproteinase, and the resulting peptides were analyzed with a nanoscale liquid chromatography-MS/MS system as described previously (22, 23). The peptide mixture was applied to a Mightysil-PR-18 (particle size, 1 μm; Kanto Chemical, Tokyo, Japan) fritless column (45 × 0.150-mm inner diameter) and fractionated over 30 min at a flow rate of 50 nl/min with a 0 to 40% gradient of acetonitrile in 0.1% formic acid. Eluted peptides were sprayed directly into a quadropole time-of-flight hybrid mass spectrometer (Q-Tof Ultima; Micromass, Manchester, UK). Mass spectrometry and MS/MS spectra were obtained in a data-dependent mode. Up to four precursor ions with an intensity above a threshold of 10 counts/s were selected for MS/MS analysis from each survey scan. All of the MS/MS spectra were compared with protein sequences in Swiss Prot and RefSeq (NCBI) with the use of batch processes of the Mascot software package (Matrix Science, London, UK). The criteria for match acceptance included the following: (i) if the match score exceeded the threshold by 10, identification was accepted without further consideration; (ii) if the difference between the score and the threshold was <10, or if a protein was identified on the basis of a single matched MS/MS spectrum, we manually confirmed the raw data before acceptance; and (iii) peptides assigned by fewer than three *y* series ions and those with a charge of +4 were eliminated regardless of their scores.

Cell Culture and Transfection—HEK293T and HeLa cells were maintained in Dulbecco's modified Eagle's medium supplemented with 10% fetal bovine serum (Invitrogen). PC12 cells were maintained in RPMI 1640 medium (Invitrogen) supplemented with 10% fetal bovine serum; they were treated with recombinant human NGF (Millipore, Billerica, MA) at 100 ng/ml in RPMI 1640 supplemented with 1% fetal bovine serum. PC12 cells were transfected with the use of a Nucleofector system (Amaxa Biosystems, Cologne, Germany), whereas other cell types were transfected with the use of the FuGENE 6 reagent (Roche Applied Science).

Antibodies—Rabbit polyclonal antibodies (for immunoblot analysis and immunoprecipitation) and a mouse monoclonal antibody (for immunofluorescence staining) specific for protrudin were generated in response to a His_6-tagged recombinant protein corresponding to amino acids 206–335 of human protrudin. A mouse monoclonal antibody to VAP-A was obtained from BD Biosciences (San Jose, CA), and rabbit polyclonal antibodies to VAP-B were kindly provided by Masaaki Matsuoka (Keio University, Japan). A mouse monoclonal antibody to glutathione *S*-transferase (GST) was obtained from MBL (Nagoya, Japan); rabbit polyclonal antibodies (H-15) to His_6 were from Santa Cruz Biotechnology (Santa Cruz, CA); antibodies to FLAG (mouse monoclonal M2 and rabbit polyclonal) and a mouse monoclonal antibody (9E10) to Myc were from Sigma; a mouse monoclonal antibody (HA11) to the HA epitope was from Research Diagnostics (Flanders, NJ); and rabbit polyclonal antibodies (HA-Y11) to HA were from Funakoshi (Tokyo, Japan). Rabbit polyclonal antibodies to calnexin were obtained from Stressgen (Victoria, Canada); a mouse monoclonal antibody to HSP90 (heat shock protein of 90 kDa) was from BD Biosciences; and a mouse monoclonal antibody to protein-disulfide isomerase (PDI) was from Affinity Bioreagents (Golden, CO). Alexa 488- or Alexa 546-conjugated goat antibodies to mouse or rabbit IgG were from Molecular Probes (Invitrogen).

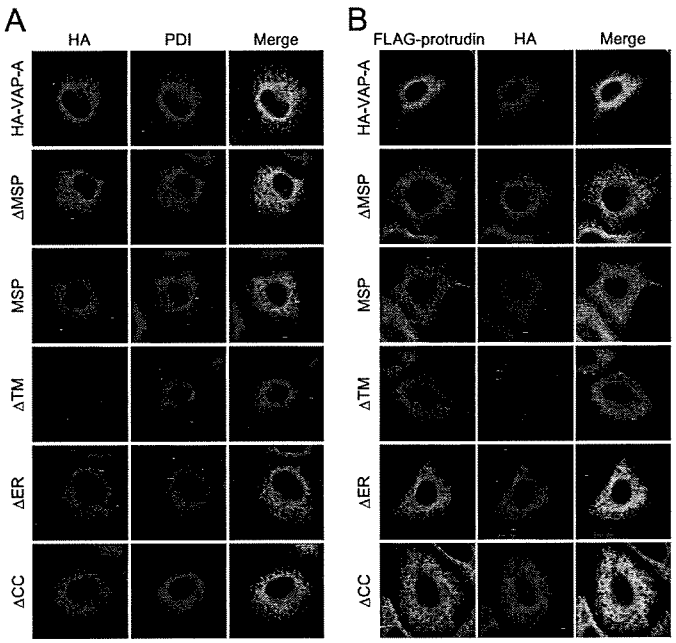

FIGURE 4. **Subcellular localization of VAP-A mutants.** *A*, HeLa cells expressing 2× HA-tagged VAP-A and deletion mutants thereof were fixed and processed for immunofluorescence analysis with anti-HA (*green*) and anti-PDI (*red*). The cells were examined with a confocal microscope. The merged images are also shown. *B*, HeLa cells expressing 3× FLAG-protrudin and 2× HA-tagged VAP-A or the indicated mutants thereof were fixed and processed for immunofluorescence staining with anti-FLAG (*green*) and anti-HA (*red*). The merged images are also shown.

Immunoblot Analysis and Immunoprecipitation—The cells were lysed in a solution containing 40 mM HEPES-NaOH (pH 7.6), 150 mM NaCl, 10% glycerol, 0.5% Triton X-100, 10 mM $MgCl_2$, 1 mM Na_3VO_4, 25 mM NaF, 1 mM phenylmethylsulfonyl fluoride, aprotinin (10 μg/ml), leupeptin (10 μg/ml), and 10 μM MG132. After incubation for 10 min at 4 °C, the lysate was centrifuged at 20,400 × *g* for 10 min at 4 °C, and the protein concentration of the resulting supernatant was determined with the Bradford assay (Bio-Rad). Whole mouse brain was homogenized by 10 strokes (900 rpm) of a Potter homogenizer in a solution containing 20 mM HEPES-NaOH (pH 7.6), 0.32 M sucrose, 1 mM Na_3VO_4, 25 mM NaF, aprotinin (10 μg/ml), leupeptin (10 μg/ml), 10 μM MG132, 1 mM phenylmethylsulfonyl fluoride, and 1 mM EDTA. The homogenate was centrifuged at 1000 × *g* for 5 min at 4 °C, and the resulting supernatant was centrifuged at 60,000 × *g* for 2 h at 4 °C. The crude microsomal pellet was resuspended in a solution containing 40 mM HEPES-NaOH (pH 7.6), 150 mM NaCl, 10% glycerol, 0.1% Triton X-100, 10 mM $MgCl_2$, 1 mM Na_3VO_4, 25 mM NaF, 1 mM phenylmethylsulfonyl fluoride, aprotinin (10 μg/ml), leupeptin (10 μg/ml), and 10 μM MG132, incubated for 10 min at 4 °C, and then centrifuged at 20,400 × *g* for 1 min at 4 °C. The protein concentration of the resulting supernatant was then determined with the Bradford assay.

The cell and mouse brain extracts were subjected to SDS-polyacrylamide gel electrophoresis, and the separated proteins

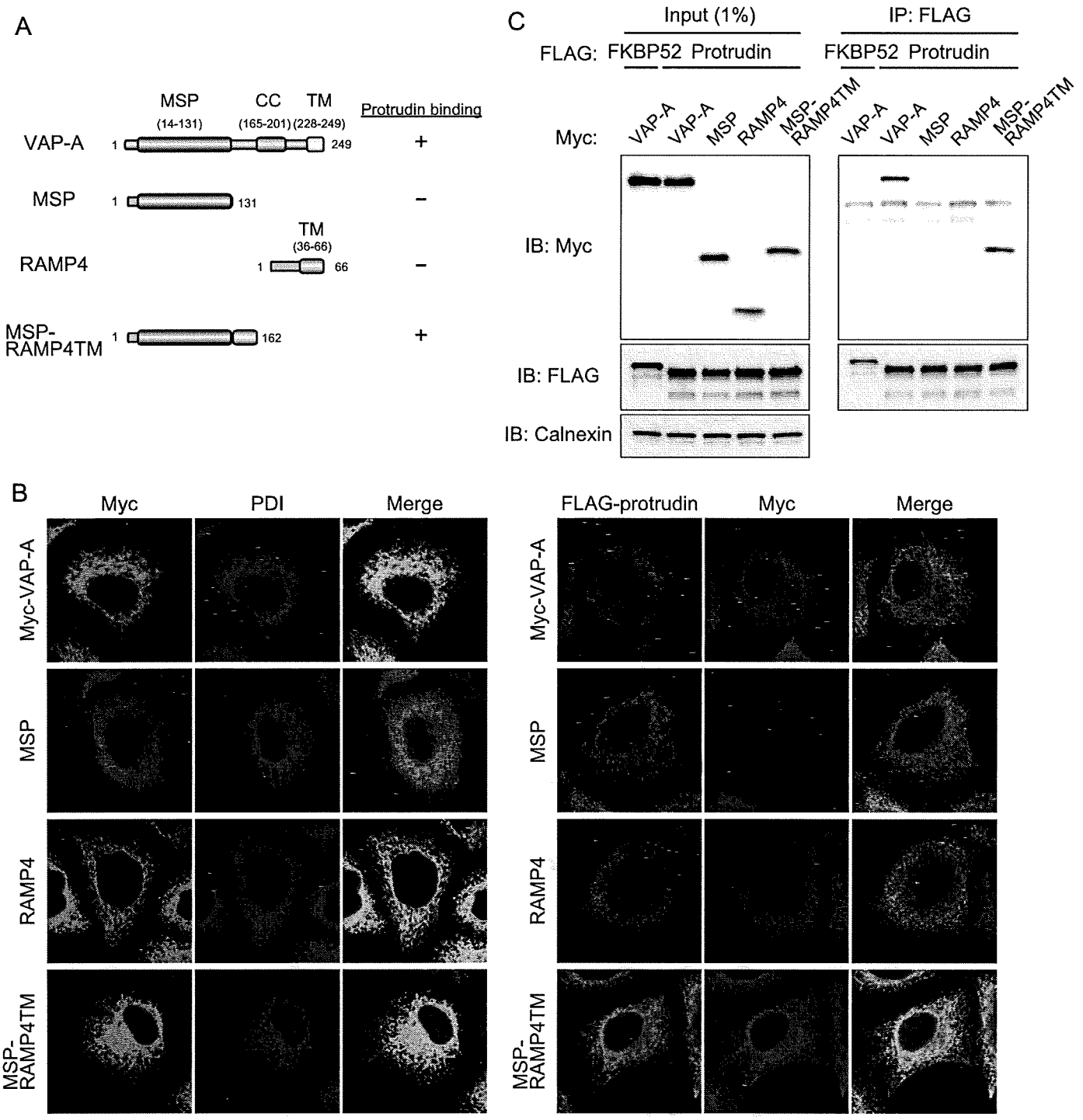

FIGURE 5. **Role of the MSP domain in the interaction of VAP-A with protrudin.** *A*, structure of human VAP-A, the MSP mutant thereof, RAMP4, and the chimeric protein MSP-RAMP4TM as well as a summary of their abilities to bind protrudin as determined in *C*. *B*, *left panel*, HeLa cells expressing 2× Myc-tagged VAP-A, MSP, RAMP4, or MSP-RAMP4TM were fixed and processed for immunofluorescence analysis with anti-Myc (*green*) and anti-PDI (*red*). The merged images are also shown. *B*, *right panel*, HeLa cells expressing 3× FLAG-protrudin and 2× Myc-tagged VAP-A, MSP, RAMP4, or MSP-RAMP4TM were fixed and processed for immunofluorescence staining with anti-FLAG (*green*) and anti-Myc (*red*). The merged images are also shown. *C*, VAP-A, MSP, RAMP4, or MSP-RAMP4TM fused at their NH_2 termini to the 2× Myc tag were expressed in HEK293T cells together with 3× FLAG-tagged protrudin or FKBP52. The cell extracts were subjected to immunoprecipitation (*IP*) with anti-FLAG, and the resulting precipitates, as well as a portion (1% of the input for immunoprecipitation) of the cell extracts, were subjected to immunoblot analysis with anti-Myc, anti-FLAG, or anti-calnexin. *IB*, immunoblot.

were transferred to an Immobilon-P membrane (Millipore) and probed with primary antibodies. Immune complexes were detected with Super Signal reagents (Thermo Scientific, Rockford, IL). For immunoprecipitation, cell or mouse brain extracts were incubated with anti-FLAG or anti-protrudin and with protein G-Sepharose 4 Fast Flow (Amersham Biosciences).

Immunofluorescence Staining—HeLa cells grown on glass coverslips were transfected with the use of the FuGENE 6 rea-

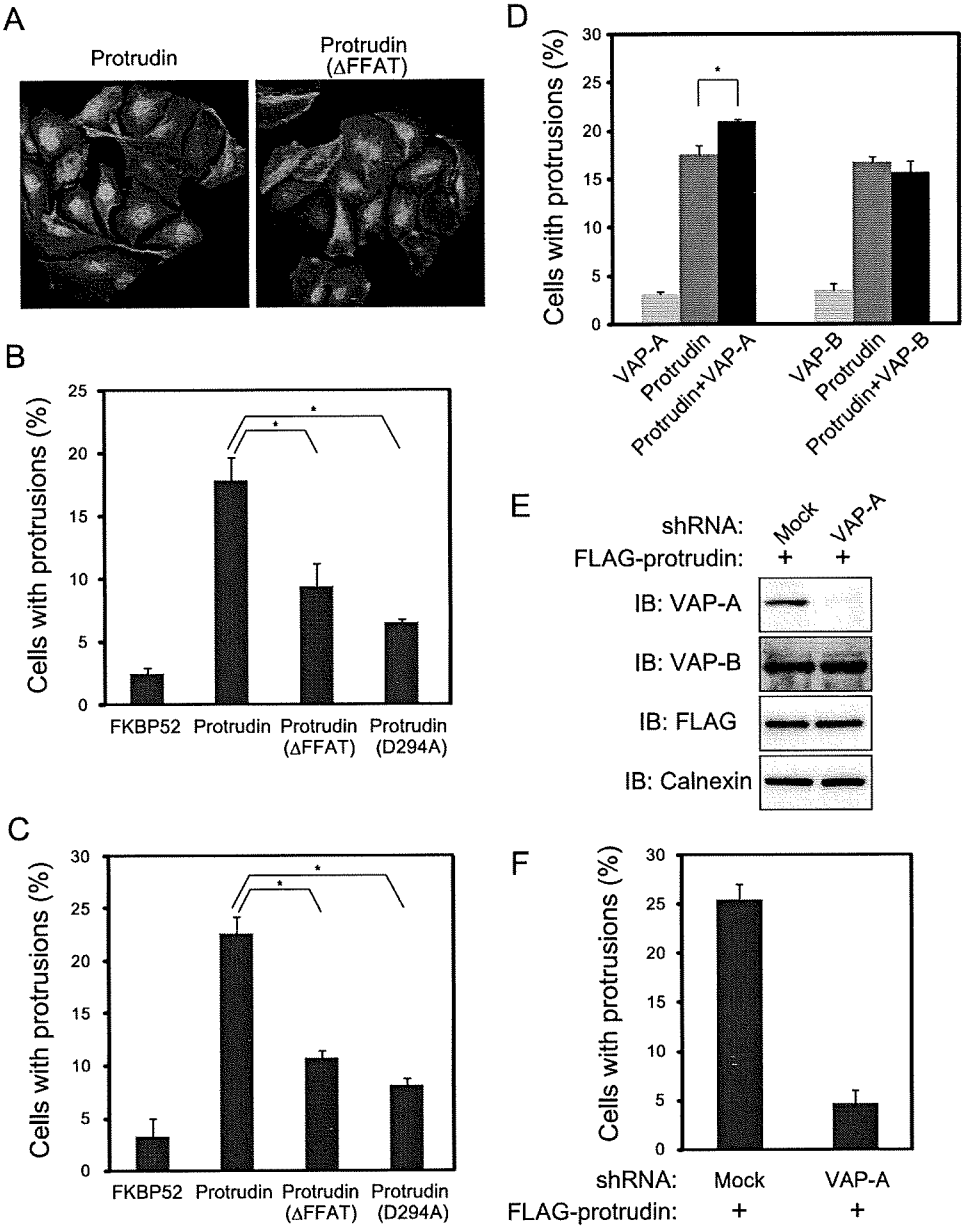

FIGURE 6. **Mutation of the FFAT motif impairs the ability of protrudin to induce process formation in HeLa cells.** *A*, HeLa cells transfected with an expression vector for 3× FLAG-tagged protrudin or the ΔFFAT mutant thereof were subjected to immunofluorescence staining with anti-FLAG (*green*). The nuclei were also stained with Hoechst 33258 (*blue*). *B* and *C*, HeLa cells transfected with expression vectors for 3× FLAG-tagged FKBP52, protrudin, protrudin(ΔFFAT), or protrudin(D294A) for 36 h (*B*) or 48 h (*C*) were stained with anti-FLAG (*green*), and the proportion of transfected cells with protrusions was determined. The data are the means ± S.E. of values from three independent experiments. $p < 0.01$ (one-way analysis of variance). *, $p < 0.05$ (Tukey-Kramer test). *D*, HeLa cells transfected with expression vectors for 3× FLAG-tagged protrudin and 2× HA-tagged VAP-A or VAP-B (or the corresponding empty vectors) were stained with anti-FLAG (*green*) or anti-HA (*red*), and the proportion of transfected cells with protrusions was determined. The data are the means ± S.E. of values from three independent experiments. *, $p < 0.005$ (Student's *t* test). *E*, HeLa cells were transfected for 48 h with an expression vector for VAP-A-shRNA 3 (or with the corresponding empty vector, pIRES-Venus-B) as well as with a vector for 3× FLAG-protrudin, after which cell extracts were subjected to immunoblot (*IB*) analysis with anti-VAP-A, anti-VAP-B, anti-FLAG, or anti-calnexin. *F*, quantitation of protrusion formation in cells treated as in *E*. The data are the means ± S.E. of values from three independent experiments. Independent experiments were performed on different days (*B–D* and *F*).

gent and subsequently prepared for immunostaining. In brief, the cells were fixed for 15 min at room temperature with 4% formaldehyde in phosphate-buffered saline (PBS) and were then incubated for 1 h at room temperature first with primary antibodies in PBS containing 0.1% bovine serum albumin and 0.1% saponin and then with Alexa 488- or Alexa 546-labeled goat secondary antibodies at a dilution of 1:2000. The cells were finally stained with Hoechst 33258 (Wako, Osaka, Japan), covered with a drop of GEL/MOUNT (Biomeda, Foster City, CA) and examined with a confocal fluorescence microscope (Radiance 2000, Bio-Rad).

Transfected PC12 cells were grown on glass coverslips coated with poly-L-lysine and subsequently prepared for immunostaining. In brief, the cells were fixed for 10 min at room temperature with 4% formaldehyde in PBS and were then incubated for 1 h at room temperature first with primary antibodies in PBS containing 0.1% bovine serum albumin and 0.1% saponin and then with Alexa 546-labeled goat secondary antibodies at a dilution of 1:2000. The cells were then covered with a drop of GEL/MOUNT and examined with a confocal fluorescence microscope (Radiance 2000).

In Vitro Binding Assay—Recombinant GST- or His_6-tagged proteins were expressed in and purified from *Escherichia coli*. Recombinant His_6-protrudin(207–409) (1 μg in 12 μl of a solution containing 20 mM Tris-HCl, pH 7.5, and 150 mM NaCl) and GST-VAP-A or mutants thereof (0.5 μg in 600 μl of a solution containing 20 mM Tris-HCl, pH 7.5, and 150 mM NaCl) were mixed and then incubated at 4 °C for 1 h with rotation. After the addition of glutathione-Sepharose 4B beads (Amersham Biosciences), the mixture was incubated for an additional 1 h at 4 °C with rotation. The beads were then washed twice with 50 volumes of Tris-buffered saline, and the bound proteins were subjected to immunoblot analysis.

Quantitation of Process Formation—Transfected cells with processes whose length was greater than the diameter of the nucleus were counted. For evaluation of the effects of FKBP52, protrudin, or protrudin mutants, the cells were immunostained with the M2 antibody to FLAG, whereas the effects of VAP-A or VAP-B were evaluated by immunostaining with the HA-Y11 antibody to HA. Ten nonoverlapping photomicrographs of each sample were examined for cell protrusion with a confocal fluorescence microscope (Radiance 2000).

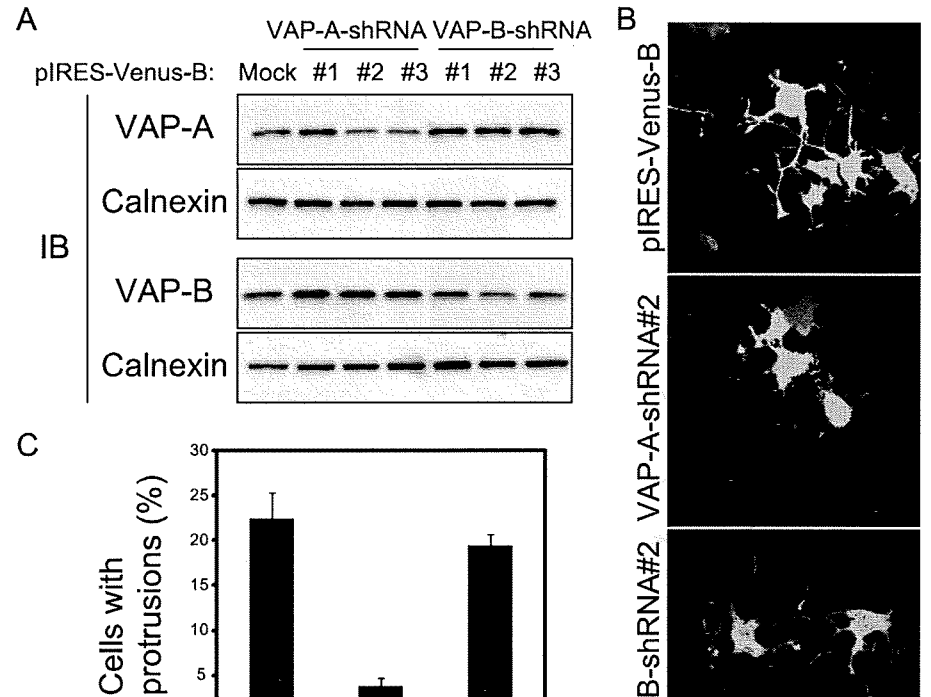

FIGURE 7. **Depletion of VAP-A results in inhibition of NGF-induced neurite outgrowth in PC12 cells.** *A*, PC12 cells were transfected with expression vectors encoding shRNAs specific for VAP-A or VAP-B mRNAs, or with the corresponding empty vector (pIRES-Venus-B), for 48 h, after which cell extracts were prepared and subjected to immunoblot (*IB*) analysis with anti-VAP-A, anti-VAP-B, or anti-calnexin. *B*, PC12 cells transfected with the indicated vectors as in *A* were stimulated with NGF for 24 h and then examined for Venus fluorescence. *C*, the proportion of transfected cells with protrusions in experiments similar to that shown in *B* was quantified. The data are the means ± S.E. of values from three independent experiments, which were performed on different days.

RESULTS

Protrudin Interacts with VAP-A via Its FFAT Motif—To investigate the physiological role of protrudin, we adopted a proteomics approach to identify proteins with which it is physically associated in cells. Human protrudin tagged with the FLAG epitope at its NH_2 terminus was expressed in HEK293T cells and then purified together with associated proteins from cell lysates by immunoaffinity chromatography with anti-FLAG. Proteins in the column eluate were digested with Lys-C endoproteinase, and the resulting peptide fragments were analyzed directly with a highly sensitive liquid chromatography-MS/MS system. The protrudin-associated proteins identified by this approach included VAP-A and VAP-B/C (Table 1).

To confirm the interaction between protrudin and VAP, we performed a coimmunoprecipitation assay. Immunoprecipitates were prepared with anti-FLAG from lysates of HEK293T cells transfected with expression vectors both for FLAG-tagged protrudin (or FLAG-tagged FKBP52 (24) as a control) and for HA-tagged VAP-A or VAP-B. We previously showed that protrudin interacts with FKBP38, but not with FKBP12 or FKBP52 (5). The resulting precipitates were then subjected to immunoblot analysis with anti-HA and anti-FLAG (Fig. 1*A*). Both VAP-A and VAP-B were detected in the immunoprecipitates prepared from the cells expressing FLAG-protrudin, but the efficiency of immunoprecipitation for VAP-A was much greater than that for VAP-B.

Similar analysis was performed to detect the potential interaction between endogenous proteins. Immunoprecipitates prepared from mouse brain extracts with anti-protrudin were subjected to immunoblot analysis with anti-VAP-A and anti-protrudin. Endogenous VAP-A was coprecipitated with endogenous protrudin (Fig. 1*B*). Together, these various data indicated that protrudin interacts with VAP-A in the physiological setting.

Given that VAP interacts with the FFAT motif of certain proteins (11, 25), we examined whether the binding of VAP-A to protrudin might be dependent on the FFAT motif of protrudin. We constructed two mutants of human protrudin, ΔFFAT and D294A (Fig. 2*A*); the former lacks the entire FFAT motif (EFKDAIE), and the latter contains Ala instead of Asp^{294}, which is required for binding of proteins to the FFAT motif (6). The amount of endogenous VAP-A associated with either mutant in HEK293T cells was greatly reduced compared with that associated with the wild-type protein, even though the expression levels of the protrudin mutants were similar to that of the wild-type protein (Fig. 2*B*). The residual interaction observed between VAP-A and the protrudin mutants was likely attributable to the fact that VAP and FFAT motif-containing proteins form a 2:2 tetramer (26), with the result that the protrudin mutants may be present in complexes of the endogenous wild-type protrudin with VAP-A. These data thus suggested that the interaction of protrudin with VAP-A is dependent on its FFAT motif.

VAP-A Interacts with Protrudin in the ER via Its MSP and TMs—VAP-A contains an major sperm protein (MSP) domain, a coiled-coil (CC) domain, and a single TM. We next investigated which of these domains are required for interaction with protrudin by generating a series of deletion mutants of VAP-A (ΔMSP29, ΔMSP59, ΔMSP89, ΔMSP, MSP, ΔTM, ΔER, and ΔCC) and examining their ability to associate with FLAG-protrudin in a coimmunoprecipitation assay (Fig. 3, *A* and *B*). Deletion of 59 amino acids from the NH_2 terminus of VAP-A (ΔMSP59) did not appear to affect its interaction with protrudin, whereas deletion of 89 amino acids from the NH_2 terminus (ΔMSP89) or of the entire MSP domain (ΔMSP) greatly reduced the efficiency of such binding. The COOH-terminal transmembrane domain of VAP-A appeared essential for the interaction with protrudin, given that the deletion mutants MSP and ΔTM did not show binding. The COOH terminus of VAP-A contains a KDEL-like sequence (KFIL), which functions as an ER retention signal (27). A mutant (ΔER) that lacks this

sequence associated with protrudin, albeit with a reduced efficiency. The coiled-coil domain, which is thought to contribute to protein-protein interaction, was not necessary for binding of VAP-A to protrudin. We also prepared a series of point mutants of VAP-A. In particular, mutation of Lys^{94} and Met^{96} (equivalent to Lys^{87} and Met^{89} of the rat protein), residues that have been shown to be critical for binding to other FFAT motif-containing proteins, attenuated (but did not abolish) the interaction between VAP-A and protrudin (Fig. 3*C*), whereas other mutations (K52N, T53A/T54A, or K125N) corresponding to residues that are important for binding of the yeast VAP homolog Scs2p to other FFAT motif-containing proteins (28) did not affect the interaction of VAP-A with protrudin.

To examine the direct interaction between VAP-A and protrudin *in vitro*, we performed a pulldown assay. Recombinant GST-tagged VAP-A and six mutants thereof were produced in bacteria and tested for their ability to bind to recombinant His_6-tagged protrudin (Fig. 3, *D* and *E*). The VAP-A mutants K94D/M96D, MSP, ΔMSP, and TM bound to protrudin, although the efficiency of binding appeared to be lower than that with full-length VAP-A. In contrast, the mutants ΔMSP/ΔTM and ΔMSP/ΔTM2 (as well as the negative controls GST and GST-RhoA) did not interact with protrudin. These results suggested that both the MSP and transmembrane domains of VAP-A are required for binding to protrudin.

The VAP-A mutant MSP did not interact with protrudin *in vivo*, although it did so *in vitro*. One possible explanation of this discrepancy was that the subcellular distribution of the VAP-A mutant differs from that of protrudin. We therefore performed immunofluorescence analysis of HeLa cells expressing various HA-tagged VAP-A constructs and FLAG-tagged protrudin. The immunofluorescence signals of wild-type VAP-A as well as of VAP-A mutants that retain an intact transmembrane domain merged with those of the ER marker protein PDI (Fig. 4*A*) (29), suggesting that they reside in the ER. These VAP-A constructs also colocalized with protrudin (Fig. 4*B*). In contrast, VAP-A mutants that lack an intact transmembrane domain (MSP and ΔTM) were distributed throughout the cytoplasm and only partially colocalized with protrudin or PDI. The distribution of protrudin appeared to be in part independent of coexpressed VAP-A mutants, probably because a substantial amount of endogenous VAP-A is present in these cells; protrudin presumably associates with the endogenous VAP-A and thereby localizes to the ER. These results thus suggested that both the MSP domain and the transmembrane domain of VAP-A contribute to the interaction with the FFAT motif of protrudin and that the transmembrane domain is also necessary for ER retention, which is a prerequisite for the interaction with protrudin.

To examine whether the MSP domain of VAP-A is intrinsically capable of interacting with protrudin *in vivo*, we generated a chimeric protein, designated MSP-RAMP4TM (Fig. 5*A*). RAMP4 is a small tail-anchored protein that exposes the NH_2 and COOH termini to the cytoplasmic and lumenal sides of the ER membrane, respectively (30). MSP-RAMP4TM was constructed by fusion of the MSP domain of VAP-A and the COOH-terminal transmembrane domain of RAMP4. Immu-

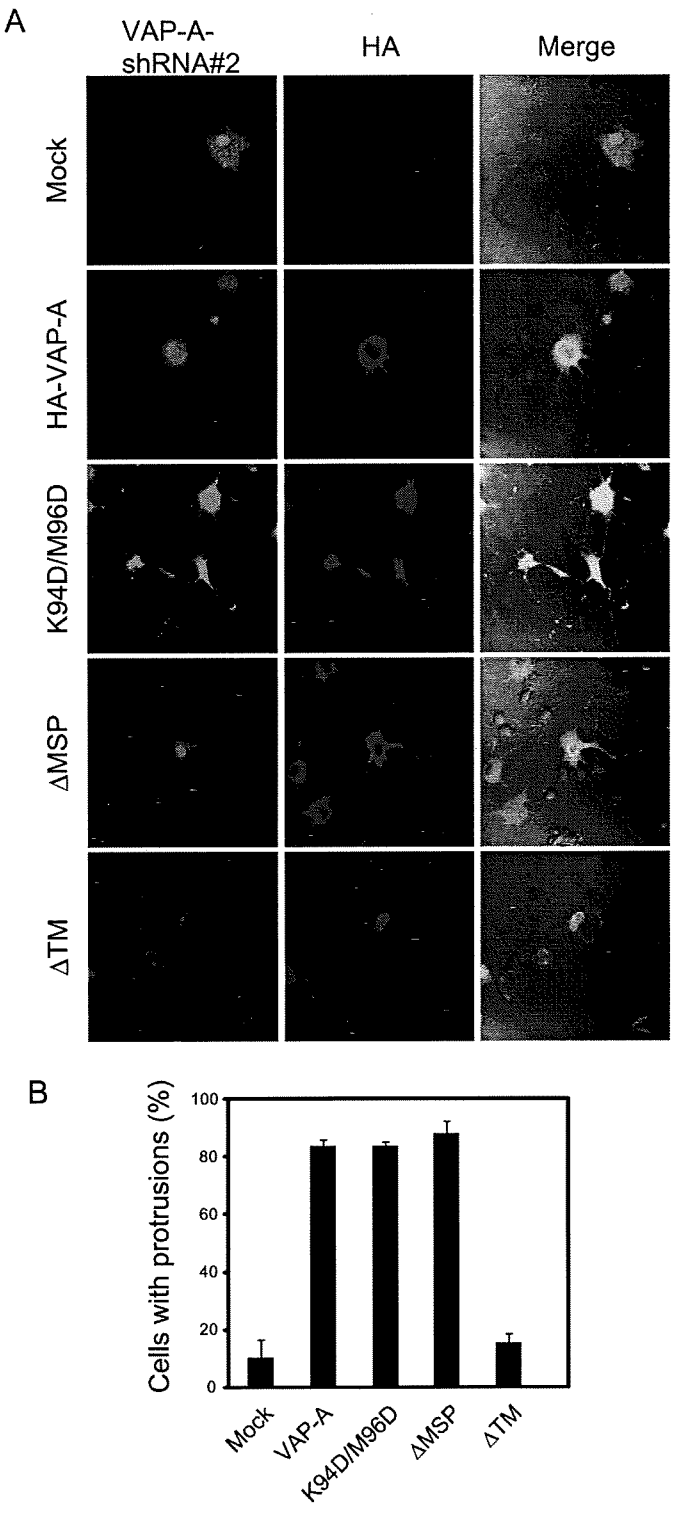

FIGURE 8. **Interaction of protrudin with VAP-A is required for NGF-induced neurite outgrowth in PC12 cells.** *A*, PC12 cells were transfected for 48 h with an expression vector encoding both VAP-A-shRNA 2 and Venus as well as with a vector for the indicated 2× HA-tagged mutants of human VAP-A, after which the cells were stimulated with NGF for 48 h and then subjected to immunofluorescence analysis with anti-HA (*red*). Venus fluorescence images (*green*) and merged images are also shown. *B*, quantitation of protrusion formation in cells treated as in *A*. The data are the means ± S.E. of values from three independent experiments, which were performed on different days.

nofluorescence analysis of HeLa cells expressing FLAG-tagged protrudin as well as Myc epitope-tagged forms of VAP-A, MSP, RAMP4, or MSP-RAMP4TM revealed that VAP-A, RAMP4, and MSP-RAMP4TM colocalized with the ER marker protein PDI (Fig. 5*B*), suggesting that these proteins reside in the ER. VAP-A and MSP-RAMP4TM also colocalized with protrudin (Fig. 5*B*). We next examined the ability of MSP-RAMP4TM to associate with protrudin in a coimmunoprecipitation assay. VAP-A and MSP-RAMP4TM interacted with protrudin, whereas MSP and RAMP4 did not (Fig. 5*C*). There results thus suggested that the MSP domain of VAP-A alone is able to interact with protrudin if it is localized to the ER. They are also consistent with the *in vitro* binding data showing that the MSP domain of VAP-A associates with protrudin in solution (Fig. 3*E*).

Mutation of the FFAT Motif Attenuates Protrudin Function—Expression of FLAG-protrudin in HeLa cells results in the generation of long processes (2) (Fig. 6*A*). To evaluate the effect of the interaction of protrudin with VAP-A on the process forming activity of protrudin, we first examined process formation in HeLa cells expressing FFAT mutants of protrudin (ΔFFAT and D294A) that have lost the ability to bind VAP-A. Protrusion was observed in <5% of cells expressing FKBP52 (negative control), whereas ~20% cells expressing wild-type protrudin showed process formation. In contrast, the efficiency of process formation was significantly reduced in cells expressing either FFAT mutant of protrudin compared with that in cells expressing the wild-type protein (Fig. 6, *A*–*C*). The residual process forming activity of the FFAT mutants was likely attributable to the formation of VAP-protrudin complexes containing both wild-type and mutant protrudin, as mentioned above. These results suggested that the FFAT motif of protrudin is necessary for the ability of the protein to induce process formation.

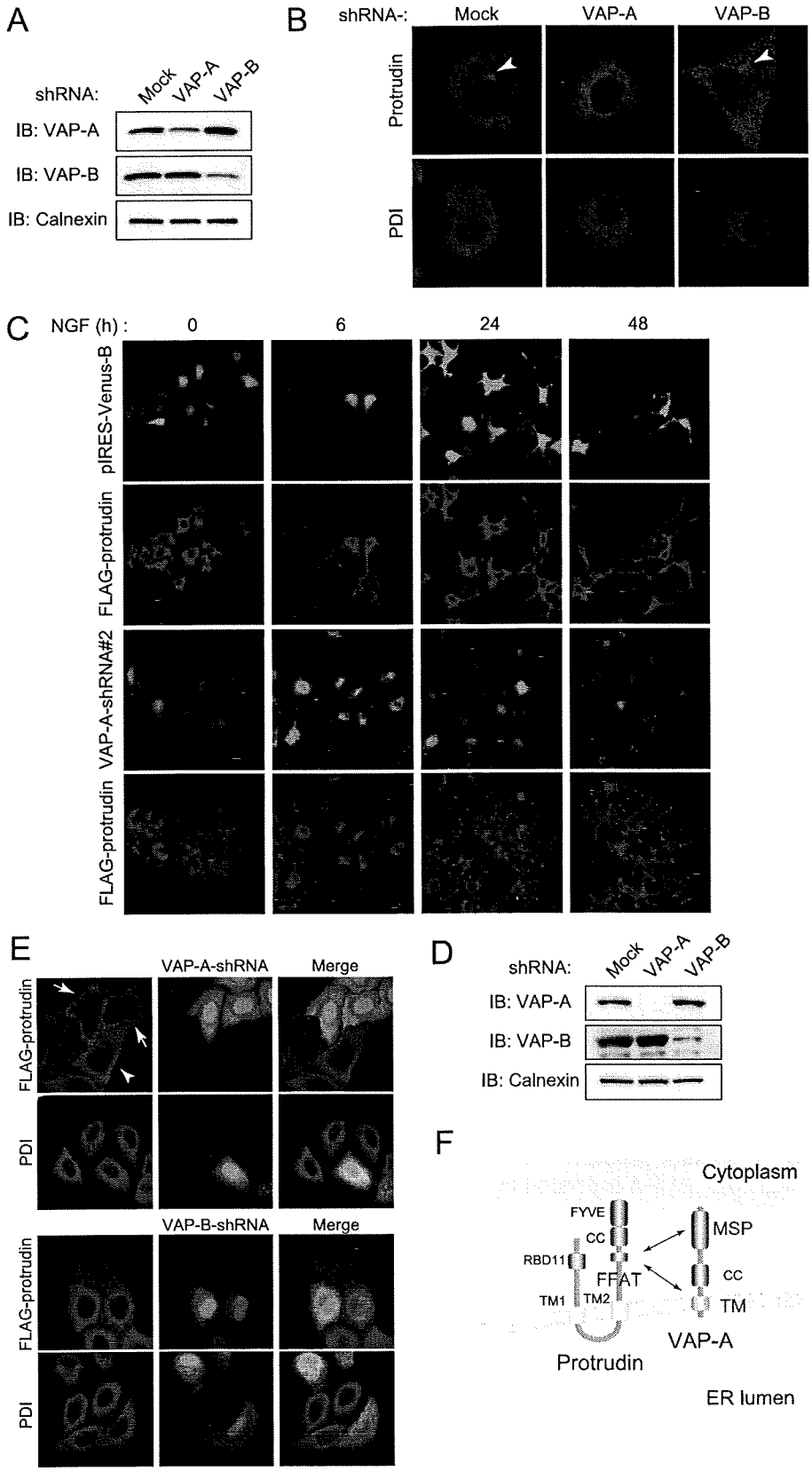

We next examined the effect of VAP overexpression on process formation. Neither VAP-A nor VAP-B alone induced process formation in HeLa cells (Fig. 6*D*). However, the expression

of VAP-A slightly but significantly increased the stimulatory effect of protrudin on process formation. VAP-B did not exhibit such an effect, consistent with the observation that the extent of binding of VAP-B to protrudin was much reduced compared with that of VAP-A (Fig. 1*A*).

We also examined the effect of VAP-A depletion on the process forming activity of protrudin by RNA interference with a VAP-A shRNA (VAP-A-shRNA 3) that targets both rat and human VAP-A mRNAs (Fig. 6*E*). Depletion of VAP-A resulted in marked inhibition of the process forming activity of protrudin (Fig. 6*F*). These results thus suggested that the interaction of protrudin with VAP-A is important for the process forming activity of protrudin.

VAP-A Is Essential for Protrudin-dependent Neurite Outgrowth—We next investigated whether VAP might be necessary for neurite extension in neurons by examining NGF-induced neurite outgrowth in PC12 cells depleted of VAP-A or VAP-B by RNA interference. Three different shRNAs specific for VAP-A mRNA or for VAP-B mRNA were tested for their ability to deplete the corresponding protein (Fig. 7*A*), and the most effective shRNAs (VAP-A-shRNA 2 and VAP-B-shRNA 2) were examined for their effects on NGF-induced neurite formation in PC12 cells. Depletion of VAP-A, but not that of VAP-B, resulted in marked inhibition of NGF-induced neurite outgrowth (Fig. 7, *B* and *C*). Moreover, depletion of VAP-A in PC12 cells eventually led to cell death (data not shown), as previously observed in rat primary neurons (31) These results thus suggested that VAP-A is essential for neurite formation and cell survival in neurons.

Given that human and rat VAP-A proteins share ~97% amino acid sequence identity, we investigated whether the defect in neurite outgrowth in PC12 cells depleted of VAP-A might be corrected by introduction of human VAP-A. Human VAP-A was resistant to shRNA-mediated interference because of a 4-nucleotide difference in the sequence corresponding to VAP-A-shRNA 2 between the human and rat mRNAs. Human VAP-A indeed restored the ability of NGF to induce neurite formation in PC12 cells that had been depleted of endogenous rat VAP-A (Fig. 8). Cell death induced by VAP-A depletion was also suppressed by expression of human VAP-A (data not shown). These results indicated that human VAP-A is functionally interchangeable with rat VAP-A.

We next tested the ability of VAP-A mutants to restore the induction of neurite outgrowth by NGF in PC12 cells depleted of endogenous VAP-A. Whereas the human VAP-A mutants K94D/M96D and ΔMSP, both of which interact with protrudin, restored NGF-induced neurite outgrowth to the same extent as did wild-type VAP-A, the mutant ΔTM, which does not reside in the ER and has lost the ability to bind to protrudin, failed to restore this effect of NGF (Fig. 8). These results suggested that the interaction of protrudin with VAP-A is likely indispensable for the neurite-extending function of protrudin. Alternatively, it remains possible that the failure of the ΔTM mutant to restore NGF-induced neurite formation in VAP-A-depleted PC12 cells might be explained by the transmembrane domain being essential for VAP-A localization and function rather than for interaction with protrudin.

VAP-A Is Required for Protrudin Localization—Protrudin resides in the ER of PC12 cells in the absence of NGF, whereas it is translocated to recycling endosomes in response to NGF stimulation (2). To investigate whether VAP-A might affect the subcellular distribution of protrudin in PC12 cells, we examined cells depleted of VAP-A or VAP-B by RNA interference (Fig. 9*A*). Immunofluorescence staining of control cells stimulated with NGF for 6 h revealed that endogenous protrudin was concentrated in the region containing recycling endosomes, whereas such transport of protrudin from the ER to recycling endosomes was not evident in cells depleted of VAP-A (Fig. 9*B*). Examination of VAP-A-depleted cells expressing FLAG-protrudin at longer times of exposure to NGF revealed that FLAG-protrudin became diffusely distributed throughout the cell body and that neurite extension was inhibited (Fig. 9*C*). In contrast, depletion of VAP-B affected neither the localization of protrudin nor neurite extension (Fig. 9*B* and data not shown). We examined the effect of VAP-A or VAP-B depletion (Fig. 9*D*) on the distribution of FLAG-protrudin in more detail in HeLa cells. Immunofluorescence corresponding to FLAG-protrudin was apparent only in the periphery of cells depleted of VAP-A, whereas it appeared to be localized to the ER in control cells and VAP-B-depleted cells (Fig. 9*E*). The localization of PDI was unaffected by VAP-A or VAP-B depletion. These results suggested that VAP-A is indispensable for ER retention of protrudin in HeLa cells, which is important for its neurite extending function.

DISCUSSION

Protrudin was discovered on the basis of its ability to induce process formation in non-neuronal cells, and this activity was shown to be essential for neurite outgrowth in neuronal cells (2, 5). Protrudin resides in the ER of neuronal cells in the absence of NGF, but it translocates to recycling endosomes in response to NGF stimulation and is ultimately transported to the tip of newly formed neurites (2). We have now investigated the molecular mechanism that underlies this translocation of protrudin by attempting to isolate proteins that interact with it and regulate its subcellular localization. Proteomics analysis led to

FIGURE 9. **Depletion of VAP-A results in an abnormal subcellular distribution of protrudin.** *A*, PC12 cells were transfected for 48 h with an expression vector for VAP-A-shRNA 2 or VAP-B-shRNA 2 or with the corresponding empty vector (pIRES-Venus-B). The cell extracts were then prepared and subjected to immunoblot (*IB*) analysis with anti-VAP-A, anti-VAP-B, or anti-calnexin. *B*, PC12 cells transfected as in *A* were stimulated with NGF for 6 h and then subjected to immunofluorescence analysis with anti-protrudin (*red*) or anti-PDI (*red*). *Arrowheads* indicate the pericentrosomal region. *C*, PC12 cells transfected as in *A* but in the additional presence of an expression vector for 3× FLAG-protrudin were stimulated with NGF for the indicated times and then subjected to immunofluorescence staining with anti-FLAG (*red*). The cells were also monitored for Venus fluorescence (*green*). *D*, HeLa cells were transfected for 48 h with an expression vector for VAP-A-shRNA 3 or for an shRNA specific for human VAP-B (or with the corresponding empty vector, pIRES-Venus-B) as well as with a vector for 3× FLAG-protrudin, after which cell extracts were subjected to immunoblot analysis with anti-VAP-A, anti-VAP-B, or anti-calnexin. *E*, HeLa cells transfected as in *D* were stained with anti-FLAG (*red*) or anti-PDI (*red*). The cells were also monitored for Venus fluorescence (*green*). *Arrows* indicate cells depleted of VAP-A (Venus positive); the *arrowhead* indicates a cell not depleted of VAP-A (Venus negative). The merged images are also shown. *F*, a model of VAP-A function in the regulation of protrudin.

the identification of VAP-A and VAP-B as proteins that interact with protrudin. These proteins are thought to regulate the localization of proteins that contain an FFAT motif through interaction with this motif (11). VAP-A and VAP-B were thus candidates for regulators of protrudin localization. Indeed, we found that VAP-A interacts with protrudin through the FFAT motif of the latter and that it is required for the ER retention of protrudin in HeLa cells. In contrast, the NGF-induced transport of protrudin from the ER to recycling endosomes in PC12 cells was shown to be dependent on VAP-A, as was the process forming activity of protrudin. Although the reason for the difference in the effects of VAP-A depletion on protrudin localization between HeLa and PC12 cells (Fig. 9, *B* and *E*) remains unclear, it might be attributable to the difference in the extent of VAP-A depletion, which was partial in PC12 cells but almost complete in HeLa cells (Fig. 9, *A* and *D*) or to a difference in the inherent properties of the two cell types. Consistent with the latter notion, VAP-A depletion eventually results in cell death in PC12 cells but not in HeLa cells (data not shown). Depletion of VAP-A also triggers cell death in primary cultured rat hippocampal neurons (31).

The FFAT motif-containing proteins CERT (11), OSBP (25), and Nir-2 (12) interact with VAP and possess lipid binding activity. The interaction of VAP with the FFAT motifs of these proteins is required for their mediation of lipid transport between intracellular membrane systems. For example, in addition to an FFAT motif, CERT contains a Start domain, which interacts with ceramide and serves to mediate ER-Golgi trafficking of ceramide. Protrudin also contains a FYVE domain, which is thought to mediate the association of proteins with phosphatidylinositol 3-phosphate (32). These common characteristics of FFAT motif-containing proteins suggest that protrudin might contribute to vesicular transport through its association with lipids in the vesicular membrane and that this role might be regulated by VAP.

The MSP domain of VAP-A has been shown to be responsible for the binding of VAP-A to the FFAT motif of its target molecules. The crystal structure of a complex of VAP-A with the FFAT motif revealed that Lys^{87} and Met^{89} of rat VAP-A are important for the interaction (26). We have now shown that the corresponding residues of human VAP-A (Lys^{94} and Met^{96}) contribute to its interaction with protrudin. In contrast, mutation of other residues of human VAP-A corresponding to those implicated in the interaction of VAP-A with the FFAT motif, including Lys^{52}, Thr^{53}, Thr^{54}, and Lys^{125}, was found not to affect the binding of human VAP-A to protrudin. However, the fact that VAP and FFAT motif-containing proteins form a 2:2 tetramer (26) makes it difficult to interpret the results of such binding analyses in cells because of the presence of the endogenous wild-type protein. In addition to the MSP domain, the transmembrane domain of VAP-A also appeared to be important for the interaction with protrudin (Fig. 9*F*). The manner of the interaction between VAP-A and protrudin may thus differ somewhat from that of the interaction between VAP-A and other FFAT motif-containing proteins.

Dysfunction of VAP or protrudin is implicated in human neurological disorders. A mutation in the MSP domain (P56S) of human VAP-B has been associated with familial amyotrophic lateral sclerosis (33, 34). This condition is characterized by the death of motor neurons in the cerebral cortex, brainstem, and spinal cord, eventually resulting in muscle weakness and atrophy followed by death caused by respiratory failure 2–5 years after disease onset. The P56S mutation affects the interaction of VAP-B with other cellular proteins (35). ZFYVE27 (protrudin) was also found to be mutated in a German family with AD-HSP, which is characterized by the selective degeneration of axons (8). The phenotype of the affected individuals is similar to that of patients with AD-HSP caused by mutation of spastin, a protein implicated in the trafficking of vesicular cargo in neurons (9). Protrudin is thought to interact with spastin via its COOH-terminal FYVE domain (8). Further molecular analysis of VAP and protrudin may thus provide insight into the pathogenesis of these neurological disorders as well as a basis for the development of new therapeutic agents.

Acknowledgments—We thank S. Nagata for vectors; A. Miyawaki for Venus cDNA; M. Matsuoka for anti-VAP-B; A. Hamasaki, N. Nishimura, and other laboratory members for technical assistance; and A. Ohta and M. Kimura for help in preparation of the manuscript.

REFERENCES

1. Zerial, M., and McBride, H. (2001) *Nat. Rev. Mol. Cell Biol.* **2,** 107–117
2. Shirane, M., and Nakayama, K. I. (2006) *Science* **314,** 818–821
3. Barik, S. (2006) *Cell Mol. Life Sci.* **63,** 2889–2900
4. Hamilton, G. S., and Steiner, J. P. (1998) *J. Med. Chem.* **41,** 5119–5143
5. Shirane, M., Ogawa, M., Motoyama, J., and Nakayama, K. I. (2008) *Genes Cells* **13,** 635–651
6. Loewen, C. J., Roy, A., and Levine, T. P. (2003) *EMBO J.* **22,** 2025–2035
7. Gillooly, D. J., Simonsen, A., and Stenmark, H. (2001) *Biochem. J.* **355,** 249–258
8. Mannan, A. U., Krawen, P., Sauter, S. M., Boehm, J., Chronowska, A., Paulus, W., Neesen, J., and Engel, W. (2006) *Am. J. Hum. Genet.* **79,** 351–357
9. Salinas, S., Carazo-Salas, R. E., Proukakis, C., Schiavo, G., and Warner, T. T. (2007) *J. Neurosci. Res.* **85,** 2778–2782
10. Hanada, K., Kumagai, K., Yasuda, S., Miura, Y., Kawano, M., Fukasawa, M., and Nishijima, M. (2003) *Nature* **426,** 803–809
11. Kawano, M., Kumagai, K., Nishijima, M., and Hanada, K. (2006) *J. Biol. Chem.* **281,** 30279–30288
12. Amarilio, R., Ramachandran, S., Sabanay, H., and Lev, S. (2005) *J. Biol. Chem.* **280,** 5934–5944
13. Kagiwada, S., Hosaka, K., Murata, M., Nikawa, J., and Takatsuki, A. (1998) *J. Bacteriol.* **180,** 1700–1708
14. Nishimura, Y., Hayashi, M., Inada, H., and Tanaka, T. (1999) *Biochem. Biophys. Res. Commun.* **254,** 21–26
15. Weir, M. L., Klip, A., and Trimble, W. S. (1998) *Biochem. J.* **333,** 247–251
16. Skehel, P. A., Fabian-Fine, R., and Kandel, E. R. (2000) *Proc. Natl. Acad. Sci. U. S. A.* **97,** 1101–1106
17. Soussan, L., Burakov, D., Daniels, M. P., Toister-Achituv, M., Porat, A., Yarden, Y., and Elazar, Z. (1999) *J. Cell Biol.* **146,** 301–311
18. Lapierre, L. A., Tuma, P. L., Navarre, J., Goldenring, J. R., and Anderson, J. M. (1999) *J. Cell Sci.* **112,** 3723–3732
19. Pennetta, G., Hiesinger, P. R., Fabian-Fine, R., Meinertzhagen, I. A., and Bellen, H. J. (2002) *Neuron* **35,** 291–306
20. Foster, L. J., and Klip, A. (2000) *Am. J. Physiol.* **279,** C877–C890
21. Shirane, M., and Nakayama, K. I. (2003) *Nat. Cell Biol.* **5,** 28–37
22. Natsume, T., Yamauchi, Y., Nakayama, H., Shinkawa, T., Yanagida, M., Takahashi, N., and Isobe, T. (2002) *Anal. Chem.* **74,** 4725–4733
23. Nakagawa, T., Shirane, M., Iemura, S., Natsume, T., and Nakayama, K. I. (2007) *Genes Cells* **12,** 709–719
24. Davies, T. H., and Sanchez, E. R. (2005) *Int. J. Biochem. Cell Biol.* **37,** 42–47

25. Wyles, J. P., McMaster, C. R., and Ridgway, N. D. (2002) *J. Biol. Chem.* **277,** 29908–29918
26. Kaiser, S. E., Brickner, J. H., Reilein, A. R., Fenn, T. D., Walter, P., and Brunger, A. T. (2005) *Structure* **13,** 1035–1045
27. Pelham, H. R. (1996) *Cell Struct. Funct.* **21,** 413–419
28. Loewen, C. J., and Levine, T. P. (2005) *J. Biol. Chem.* **280,** 14097–14104
29. Freedman, R. B., Hirst, T. R., and Tuite, M. F. (1994) *Trends Biochem. Sci.* **19,** 331–336
30. Favaloro, V., Spasic, M., Schwappach, B., and Dobberstein, B. (2008) *J. Cell Sci.* **121,** 1832–1840
31. Teuling, E., Ahmed, S., Haasdijk, E., Demmers, J., Steinmetz, M. O., Akhmanova, A., Jaarsma, D., and Hoogenraad, C. C. (2007) *J. Neurosci.* **27,** 9801–9815
32. Takenawa, T., and Itoh, T. (2006) *IUBMB Life* **58,** 296–303
33. Nishimura, A. L., Mitne-Neto, M., Silva, H. C., Richieri-Costa, A., Middleton, S., Cascio, D., Kok, F., Oliveira, J. R., Gillingwater, T., Webb, J., Skehel, P., and Zatz, M. (2004) *Am. J. Hum. Genet.* **75,** 822–831
34. Kanekura, K., Nishimoto, I., Aiso, S., and Matsuoka, M. (2006) *J. Biol. Chem.* **281,** 30223–30233
35. Mitne-Neto, M., Ramos, C. R., Pimenta, D. C., Luz, J. S., Nishimura, A. L., Gonzales, F. A., Oliveira, C. C., and Zatz, M. (2007) *Protein Expression Purif.* **55,** 139–146

J. Biochem. 2009;145(5)565–573
doi:10.1093/jb/mvp016

Impaired chemotaxis and cell adhesion due to decrease in several cell-surface receptors in cathepsin E-deficient macrophages

Takayuki Tsukuba[1,*], Michiyo Yanagawa[2], Kuniaki Okamoto[1], Yoshiko Okamoto[3], Yoshiyuki Yasuda[4], Keiichi I. Nakayama[5], Tomoko Kadowaki[6] and Kenji Yamamoto[7]

[1]Department of Dental Pharmacology, Graduate School of Biomedical Sciences, Nagasaki University, Nagasaki 852-8588; [2]Department of Fixed Prosthodontics, Graduate School of Dental Science, Kyushu University, Fukuoka 812-8582; [3]Department of Biochemistry, Daiichi University College of Pharmaceutical Sciences, Fukuoka 815-8511; [4]Division of Clinical Cariology and Endodontology, Department of Oral Rehabilitation, School of Dentistry, Health Sciences University of Hokkaido, Hokkaido, 061-0293; [5]Department of Molecular and Cellular Biology, Medical Institute of Bioregulation, Kyushu University, Fukuoka 812-8582; [6]Pharmacology, Graduate School of Dental Science, Kyushu University, Fukuoka 812-8582; and [7]Proteolysis Research Laboratory, Graduate School of Pharmaceutical Sciences, Kyushu University, Fukuoka 812-8582, Japan

Received November 26, 2008; accepted January 9, 2009; published online January 27, 2009

Cathepsin E is an endo-lysosomal aspartic proteinase exclusively present in immune system cells. Previous studies have shown that cathepsin E-deficient ($CatE^{-/-}$) mice display aberrant immune responses such as atopic dermatitis and higher susceptibility to bacterial infection. However, the mechanisms underlying abnormal immune responses induced by cathepsin E deficiency are still unclear. In this study, we found that the cell-surface levels of chemotactic receptors, including chemokine receptor (CCR)-2 and *N*-formyl peptide receptors (FPRs), were clearly diminished in $CatE^{-/-}$macrophages compared with those in wild-type cells. Consistently, chemotaxis of $CatE^{-/-}$macrophages to MCP-1 and *N*-formyl-methionyl-leucyl-phenylalanine was also decreased. Similar to the chemotactic receptors, the surface expressions of the adhesion receptors CD18 (integrin β_2) and CD 29 (integrin β_1) in $CatE^{-/-}$ macrophages were significantly decreased, thereby reducing cell attachment of $CatE^{-/-}$ macrophages. These results indicate that the defects in chemotaxis and cell adhesion are likely to be involved in the imperfect function of $CatE^{-/-}$macrophages.

Key words: aspartic proteinase, cathepsin E, knockout, macrophages, chemotaxis, cell adhesion.

Abbreviations: $CatE^{-/-}$, cathepsin E-deficient; CCR-2, chemokine receptor; FITC, fluorescein isothiocyanate; FPRs, *N*-formyl peptide receptors; LAMP, lysosome-associated membrane protein; MCP, monocyte chemoattractant protein; PBS, phosphate buffered saline; PE, phycoerythin; TLRs, toll-like receptors.

Cathepsin E (EC 3.4.23.34) is an intra-cellular aspartic proteinase, which is mainly localized in the endosomal/lysosomal compartments within cells (*1–3*). Since cathepsin E is predominantly expressed in immune-related cells, including macrophages, dendritic cell, and microglia, this enzyme has been speculated to be involved in the proteolysis of endosomal/lysosomal compartments in immune-related cells (*4–6*). We have previously generated cathepsin E-deficient ($CatE^{-/-}$) mice that spontaneously developed atopic dermatitis-like skin lesions when reared under conventional conditions but not under specific pathogen-free conditions (*7*). These results imply that development of this disorder in these mice appeared to be triggered by some environmental factor(s) such as pathogenic micro-organisms. Thereafter, we showed that $CatE^{-/-}$ mice exhibit increased susceptibility to infection with bacteria such as *Staphylococcus aureus* and *Porphyromonas gingivalis* (*8*). However, the molecular mechanisms inducing aberrant immune responses in $CatE^{-/-}$ mice remain to be elucidated.

Recently, we demonstrated that peritoneal macrophages derived from $CatE^{-/-}$ mice display a novel type of lysosomal storage disorder characterized by the accumulation of major lysosomal membrane sialoglycoproteins, such as lysosome-associated membrane protein (LAMP)-1 and LAMP-2, in the cells with a concomitant elevated lysosomal pH (*9*). Since an elevated pH is known to induce abnormal properties of endolysosomal compartments including abnormal processing and targeting of lysosomal proteins (*10*, *11*) and abnormal maturation and/or fusion events of the acidic organelles (*12*), $CatE^{-/-}$ macrophages are assumed to show trafficking defects in both membrane and soluble proteins. Indeed, we found the enhanced secretion of soluble lysosomal enzymes by $CatE^{-/-}$ macrophages (*9*). In addition to soluble proteins, we reported decreased surface levels of Toll-like receptors (TLRs), which are capable of recognizing specific components of micro-organisms, in $CatE^{-/-}$ macrophages, further we reported diminished cytokine production by $CatE^{-/-}$ macrophages that are stimulated by specific TLR ligands (*8*). However, no information is available concerning the

*To whom correspondence should be addressed. Tel: +81 95 819 7652, Fax: +81 95 819 7655, E-mail: tsuta@nagasaki-u.ac.jp

trafficking defects of receptors other than TLRs on the cell surface of $CatE^{-/-}$ macrophages.

Macrophages express a large number of cell surface receptors, which recognize a wide range of specific endogenous and exogenous ligands (*13*). Among them, chemotactic receptors play an important role in immune responses (*14*). Recognition of chemoattractants by chemotactic receptors, which is known as chemotaxis, regulates leucocyte recruitment to sites of inflammation and infection (*15*, *16*). The chemotactic receptors belong to the 7-transmembrane-G-protein-coupled receptor family, and trigger various immune responses besides chemotaxis, induce the production of reactive oxygen species and stimulate the release of proteolytic enzymes from granules, in the case of neutrophils (*17*). Concerning chemotactic responses, we have more recently reported that bone-marrow-derived macrophages from $CatE^{-/-}$ mice display impaired chemotaxis in responses to a chemokine and a bacterial peptide (*18*). However, precise mechanisms of the diminished chemotaxis in $CatE^{-/-}$ macrophages remain unknown. In addition to chemotactic receptors, leucocyte recruitment to inflammatory and infectious sites is orchestrated by cell-adhesion molecules (*19*). Cell-adhesion receptors are surface proteins involved in the binding of cells with other cells or the extra-cellular matrix (*20*, *21*). The cell-adhesion receptors belong to four major families, namely, the immunoglobulin superfamily, the cadherins, the selectins and the integrins (*22*). In particular, the integrins, which are heterodimers formed by the two non-covalent linking two subunits α and β, are also involved in various intra-cellular signalling pathways as well as in cell attachment (*20*, *23*). Therefore, it is of importance to investigate whether or not the chemotactic receptors and cell-adhesion receptors on the cell surface of $CatE^{-/-}$ macrophages are decreased.

In this study, we focused on chemotaxis and cell adhesion in $CatE^{-/-}$ macrophages, and observed impaired chemotaxis and cell-adhesion ability in them with concomitant decreased surface levels of chemotactic receptors and cell-adhesion receptors compared with those in wild-type cells.

MATERIALS AND METHODS

Materials—RPMI-1640, fluorescein dextran (70,000 MW) and fluorescein-conjugated chemotactic hexapeptide *N*-formyl-Nle-Leu-Phe-Nle-Tyr-Lys were purchased from Invitrogen, Japan. Anti-mouse LAMP-1 and LAMP-2 antibodies were purchased from Southern Biotechnology Inc (Birmingham, AL, USA). Anti-mouse CCR2 monoclonal antibody conjugated with phycoerythin (PE) was purchased from R& D Systems Inc. Anti-mouse CD18 and CD29 monoclonal antibodies conjugated with fluorescein isothiocyanate (FITC) were purchased from BD Biosciences.

Mice—Wild-type and $CatE^{-/-}$ mice with the C57BL/6 genetic background were used as described previously (*9*). Animals were maintained under specific pathogen-free conditions according to the guidelines of the Japanese Pharmacological Society. Animals and all experiments were approved by the Animal and Microbiological Research Committee of the Graduate School of Dental Science, Kyushu University. All experiments were performed with age-matched, male $CatE^{-/-}$ mice and wild-type littermates.

Preparation of Peritoneal Macrophages—Thioglycolate-elicited peritoneal macrophages were isolated as described previously (*9*). Briefly, 8–14-week-old mice were peritoneally injected with 4.05% thioglycolate (2 ml/mouse). Three and a half days later, peritoneal exudate cells were isolated from the peritoneal cavity by washing with phosphate buffered saline (PBS). The cells were incubated in RPMI 1640 medium supplemented with 10% penicillin (50 U/ml) and streptomycin (50 μg/ml) at 37°C with 5% CO_2. After incubation for 2 h, floating cells were removed by washing three times with Ca^{2+}/Mg^{2+}-free PBS. MAC-2-positive macrophages comprised more than 95% of the isolated cells.

Cell Staining and Flow Cytometry—The peritoneal macrophage suspension (2×10^5 cells/100 μl) was incubated on ice for 15 min with primary antibodies appropriately diluted with PBS containing 2.5% fetal bovine serum (FBS) and 0.01% NaN_3 (buffer A). Samples were pre-incubated with Fc Block (anti-mouse CD16/CD32 antibody) (BD Pharmigen), and subsequently with specific antibodies or control antibodies conjugated with PE or FITC for 15 min on ice. In case of permeabilization, cells were prepared by treatment with 0.03% saponin in buffer A for 15 min on ice. Flow cytometric analyses were performed on a Beckman Coulter Epics XL cytometer.

Cell-Adhesion Assay—Fibronectin (20 μg/ml) in RPMI medium or untreated medium (uncoated) was added in a 96-well plate, and incubated overnight at 4°C. The wells were blocked with RPMI medium containing 0.5% bovine serum albumin (BSA). After washing with RPMI medium containing 0.1% BSA (washing buffer), peritoneal macrophages (5×10^5 cells) were added to each well and incubated at 37°C for 10, 20 or 30 min. Floating or weakly bound cells in the plate were gently removed by filling the wells three times with washing buffer. Bound cells were fixed with 4% paraformaldehyde in PBS for 10 min. After washing, cells were stained with 50 μl of crystal violet (5 mg/ml in 2% ethanol). After washing three times with the washing buffer, the stained plate was assayed with a microplate reader at 540 nm.

Chemotactic Assay—Chemotactic assay was performed as described previously (*18*). Briefly, peritoneal macrophages (2×10^5 cells/ml) were washed and re-suspended in RPMI medium. Migration of cells in response to the medium alone, MCP-1 or fMLP was assessed in a 24-well chemotaxis chamber separated by polyethylene terephthalate membrane (pore size, 5 μm). The macrophages were loaded into the upper chambers and tested for chemoattraction to the media alone (RPMI-1640 medium without FBS as a control medium), MCP-1(0.1 nM) or fMLP (1 μM). The chambers were incubated at 37°C in 5% CO_2 for 90 min. The cells that migrated into the lower wells were fixed with 4% paraformaldehyde in PBS for 10 min; subsequently stained with May-Giemsa, and then counted by light microscopy.

Endocytosis Assay—Peritoneal macrophages (5×10^6 cells) were incubated with fluorescein dextran (20 μg/ml) in normal RPMI-1640 medium containing 10% FBS

for 30 or 60 min. After washing with PBS containing 1 mg/ml of BSA, cells were lysed in 50 mM Tris–HCl buffer (pH 8.5) containing 0.1% Triton X-100. The amounts of fluorescence in the cell lysates were measured by spectrofluorometry (Hitachi 650-40) and normalized to the total cell protein levels.

Statistical Analysis—The statistical significance of differences was determined using the Student's *t*-test.

RESULTS

Impaired Chemotaxis and Decreased Cell-Surface Levels of Chemotactic Receptors in CatE$^{-/-}$ Macrophages—During a series of experiments that we performed, we had assumed that the number of thioglycolate-elicited peritoneal macrophages in CatE$^{-/-}$ mice was possibly lower than that in the wild-type mice. Therefore, we accurately measured the number of thioglycolate-elicited peritoneal macrophages in the wild-type and CatE$^{-/-}$ mice. The number of peritoneal macrophages in the CatE$^{-/-}$ mice was significantly lower than that in the wild-type mice (Fig. 1), suggesting that chemotaxis or other chemotactic factor(s) might be more impaired in the CatE$^{-/-}$ mice than in the wild-type mice.

Recently, we reported that chemotactic responses of the bone-marrow-derived macrophages acquired from CatE$^{-/-}$ mice were significantly decreased compared with those from wild-type mice, whereas no marked differences were observed in the responses of bone-marrow-derived dendritic cells acquired from wild-type and CatE$^{-/-}$ mice (*18*). To further investigate the chemotaxis of peritoneal macrophages, we determined the chemotactic responses of wild-type and CatE$^{-/-}$ macrophages to the typical chemokine monocyte chemoattractant protein (MCP)-1. The number of CatE$^{-/-}$ macrophages that migrated from the upper to the lower chamber in response to MCP-1 was lower than that of the wild-type macrophages (Fig. 2). Similar results were observed in experiments with a bacterial-derived chemoattractant, *N*-formyl-methionyl-leucyl-phenylalanine (fMLP) (Fig. 2). These results of peritoneal macrophages in this study were quite consistent with previous results obtained with those of bone-marrow-derived macrophages (*18*). In addition, we have investigated chemotaxis of resident peritoneal macrophages that were not activated by thioglycolate from wild-type and CatE$^{-/-}$ mice in response to MCP-1 and fMLP. However, the results of resident macrophages were essentially similar to those of thioglycolate-activated macrophages (data not shown).

To evaluate the cell-surface levels of chemotactic receptors on the wild-type and CatE$^{-/-}$ macrophages, we analysed the surface expression of CCR2, which is the receptor for MCP-1, and *N*-formyl peptide receptors (FPRs), which are the receptors for several FPRs including fMLP, by flow cytometry. As shown in Fig. 3A,

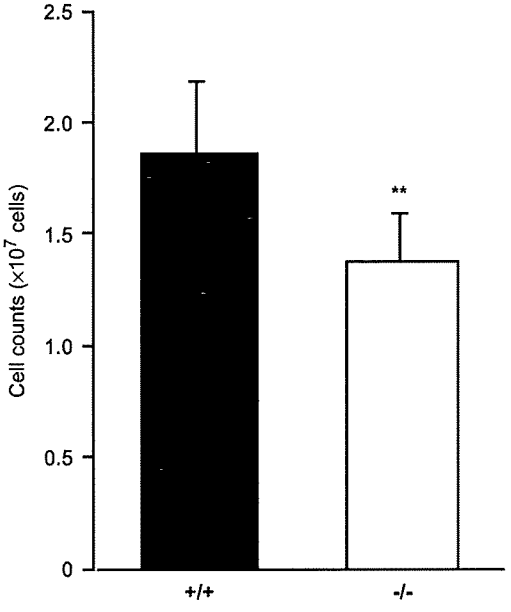

Fig. 1. **Number of thioglycolate-elicited peritoneal macrophages derived from wild-type or CatE$^{-/-}$ mice.** Mice were peritoneally injected with 4.05% thioglycolate (2 ml/mouse). Three and half days later, peritoneal exudate cells were isolated from the peritoneal cavity by washing with PBS. The cells were incubated with RPMI medium containing 10% FBS at 37°C for 2 h, and subsequently washed three times with PBS. After removing cells with trypsin, the cell number was determined by light microcopy using Burker-Turk hemocytometer chambers. The data are means ± SD for five independent experiments. $^{**}P < 0.01$, *vs.* the corresponding values for the wild-type littermates, obtained with the unpaired Student's *t*-test.

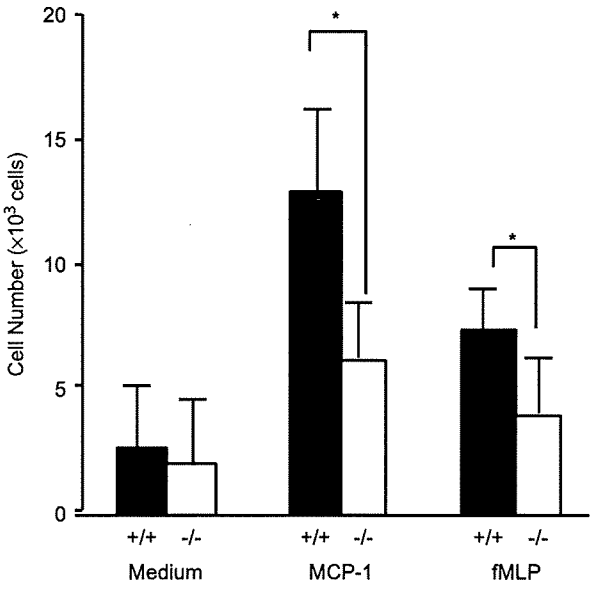

Fig. 2. **Chemotaxis of peritoneal macrophages from wild-type or CatE$^{-/-}$ mice in response to MCP-1 and fMLP.** Peritoneal macrophages were washed and re-suspended in RPMI-1640 medium without FBS as a control medium. Migration of cells in response to a concentration of MCP-1 (0.1 nM) and fMLP (1 μM) was assessed in a 24-well Transwell chemotaxis chamber. The chambers were incubated at 37°C for 90 min. The cells that migrated to the lower well were fixed, subsequently stained with trypan blue and then counted by light microscopy. The data are means ± SD for five independent experiments. $^{*}P < 0.05$, *vs.* the corresponding values for the wild-type macrophages, obtained with the unpaired Student's *t*-test.

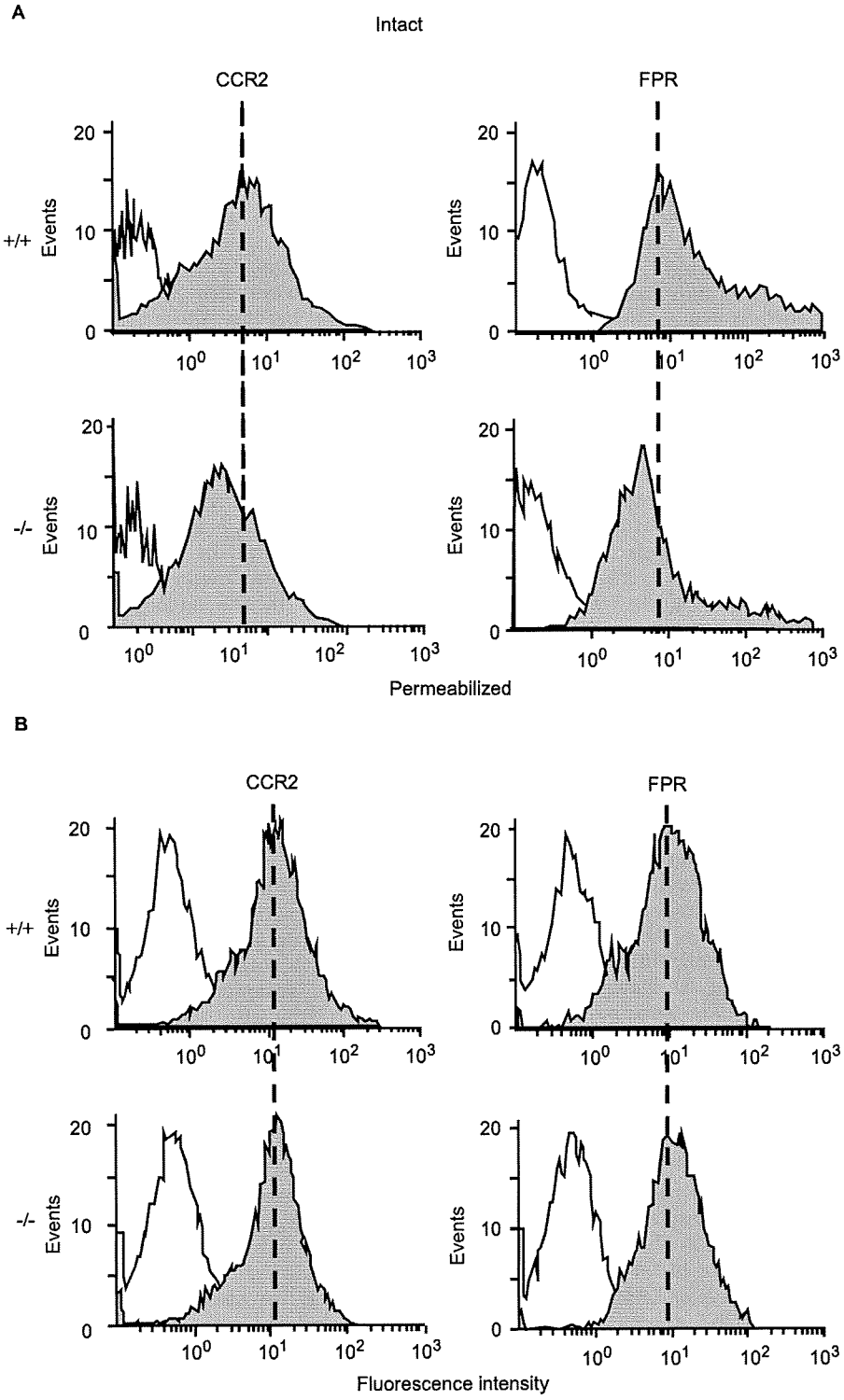

Fig. 3. **Flow cytometric analysis of expression levels of CCR2 and FPRs in wild-type or *CatE*$^{-/-}$ macrophages.** (A) Peritoneal macrophages (2×10^5 cells) from wild-type and *CatE*$^{-/-}$ mice were stained for cell surface with a specific antibody for CCR2 conjugated with PE, or with *N*-formyl-Nle-Leu-Phe-Nle-Tyr-Lys-fluorescein, and then analysed by flow cytometry. Data are representative of five independent experiments. (B) The cells were permeabilized with saponin, and then stained for determination of the total expression levels of CCR2 or FPRs. Data are representative of five independent experiments.

CatE$^{-/-}$ cells showed decreased levels of both CCR2 and FPR as compared with wild-type cells. However, this difference in receptor levels was abrogated with permeabilized cells that were pre-treated with saponin, which enabled the detection of both intra-cellular and extracellular expression of proteins, indicating that the total levels of expression of CCR2 and FPRs between the two cell types were comparable (Fig. 3B).

Reduced Cell-Adhesion Ability and Decreased Cell-Surface Levels of Cell-Adhesion Receptors in CatE$^{-/-}$ *Macrophages*—To further examine the cell-surface levels of receptors other than TLRs and chemotactic receptors, we investigated the surface expressions of cell-adhesion receptors in peritoneal macrophages from wild-type and *CatE*$^{-/-}$ mice. Integrins are major cell-adhesion receptors; they are heterodimers composed of α and β subunits (*23*). When we analysed the cell-surface expression of CD18 (integrin β_2 chain) on wild-type and *CatE*$^{-/-}$ macrophages by flow cytometry, we observed that the surface expression of CD18 was reduced in *CatE*$^{-/-}$ macrophages compared with those of the wild-type cells (Fig. 4A). Similarly, the surface levels of CD29 (integrin β_1 chain) on *CatE*$^{-/-}$ macrophages were more decreased than those of wild-type cells (Fig. 4A). However, treatment with saponin showed no significant difference in the total expression levels of receptors between wild-type and *CatE*$^{-/-}$ macrophages (Fig. 4B). These results indicate that the surface levels of cell-adhesion receptors were also decreased in *CatE*$^{-/-}$ macrophages in spite of the similarity in the total expression levels of receptors between wild-type and *CatE*$^{-/-}$ macrophages.

To test the adhesion abilities of wild-type and *CatE*$^{-/-}$ macrophages, we analysed the attachment of cells to uncoated or fibronectin-coated plastic plates. It is known that both CD18 and CD29 are involved in the interaction of these cells with plastics or fibronectin (*24*). At an early incubation time of 10 or 20 min, the density of bound *CatE*$^{-/-}$ macrophages was significantly lower than that of wild-type macrophages (Fig. 5). However, at a longer incubation time of 30 min, there were no marked differences in the cell density between wild-type and *CatE*$^{-/-}$ macrophages (Fig. 5A). When we analysed the adhesion of macrophages to fibronectin-coated plates, we observed the density of attached *CatE*$^{-/-}$ macrophages to be diminished more than that of wild-type macrophages at 10 or 20 min of incubation (Fig. 5B). Taken together with the results of the adhesion assay and the flow cytometric analysis, the reduced cell-adhesion ability in *CatE*$^{-/-}$ macrophages is probably due to the decreased surface levels of cell-adhesion receptors in *CatE*$^{-/-}$ cells.

Decreased Cell-Surface Levels of LAMP-1 and LAMP-2 in CatE$^{-/-}$ *Macrophages*—Our previous study showed that cathepsin E deficiency induces accumulation of LAMP-1 and LAMP-2 in the immune system cells (*9*). On the other hand, it is known that LAMPs are mainly localized in the limiting membranes of lysosomes and late endosomes; however, small amounts of LAMPs are also detectable on the cell surface (*25*, *26*). Therefore, we assumed the possibility that the accumulation of LAMP-1 and LAMP-2 within the cells due to cathepsin E deficiency might cause decreased surface amounts of these lysosomal membrane proteins. We subsequently compared the surface levels of LAMPs between wild-type and *CatE*$^{-/-}$ macrophages. As shown in Fig. 6, flow cytometric analysis revealed that the surface levels of LAMP-1 and LAMP-2 were notably lower than those of wild-type cells. In contrast, treatment with saponin showed that the total expression levels of *CatE*$^{-/-}$ macrophages were higher than those of wild-type cells (data not shown). The data are consistent with previous data obtained with western blot or flow cytometric analysis performed to evaluate LAMP-1 and LAMP-2 expression (*9*, *18*). Thus, the surface expressions of LAMP-1 and LAMP-2 were also decreased in *CatE*$^{-/-}$ macrophages, probably because these lysosomal proteins accumulated in endosomes and lysosomes in *CatE*$^{-/-}$ cells (*9*).

Normal Endocytosis of FITC-Dextran in CatE$^{-/-}$ *Macrophages*—We finally examined whether cathepsin E deficiency might affect the vesicle transport, including endocytosis, in addition to the membrane transport to the cell surface. We subsequently analysed endocytosis in macrophages with FITC-dextran. After incubation at 30 or 60 min, we measured the intra-cellular amounts of FITC-dextran in wild-type and *CatE*$^{-/-}$ macrophages by spectrofluorometry. However, there was no notable difference in the endocytic efficiency of FITC-dextran between wild-type and *CatE*$^{-/-}$ macrophages (Fig. 7). We also found no significant difference between the endocytosis of wild-type and *CatE*$^{-/-}$ macrophages at 24 h of incubation time (data not shown). Therefore, it appears probable that the cathepsin E deficiency causes membrane-trafficking defects, but not vesicle-trafficking defects such as endocytosis.

DISCUSSION

This study indicates that surface levels of CCR2 and FPRs chemotactic receptors, and CD18 and CD29 adhesion receptors were decreased in *CatE*$^{-/-}$ macrophages. Consistent with the reduced levels of chemotactic and adhesion receptors, the chemotactic and cell-adhesion ability were also defective in *CatE*$^{-/-}$ macrophages. In addition to surface proteins, the surface levels of LAMP-1 and LAMP-2 were diminished in *CatE*$^{-/-}$ macrophages. However, the endocytosis of dextran in wild-type and *CatE*$^{-/-}$ macrophages was indistinguishable. Thus, the membrane trafficking of some receptors and membrane proteins to the cell surface and their functions were partially defective in *CatE*$^{-/-}$ macrophages.

Our previous study has shown that cathepsin E deficiency induces accumulation of LAMP-1 and LAMP-2 accompanied by an elevation of lysosomal pH (*9*). Moreover, we have reported that the surface levels of TLR2 and TLR4 are decreased in *CatE*$^{-/-}$ macrophages; further we have reported that their cytokine production by *CatE*$^{-/-}$ macrophages in response to the specific TLR2 ligand (peptideglycan) and the TLR4 ligand (lipopolysaccharide) is diminished (*8*). However, this study demonstrated that surface levels of not only TLR, but also the chemotactic receptors and the adhesion receptors were decreased in *CatE*$^{-/-}$ macrophages. Importantly this study showed that the surface levels of LAMP-1 and LAMP-2 were also diminished in *CatE*$^{-/-}$ macrophages. Thus, cell-surface receptors and the surface expression of